

Compositional maps for registration in complex geometries

Tommaso Taddei¹

¹ Univ. Bordeaux, CNRS, Bordeaux INP, IMB, UMR 5251, F-33400 Talence, France

Inria Bordeaux Sud-Ouest, Team MEMPHIS, 33400 Talence, France,

tommaso.taddei@inria.fr

Abstract

We develop and analyze a parametric registration procedure for manifolds associated with the solutions to parametric partial differential equations in two-dimensional domains. Given the domain $\Omega \subset \mathbb{R}^2$ and the manifold $\mathcal{M} = \{u_\mu : \mu \in \mathcal{P}\}$ associated with the parameter domain $\mathcal{P} \subset \mathbb{R}^P$ and the parametric field $\mu \mapsto u_\mu \in L^2(\Omega)$, our approach takes as input a set of snapshots from \mathcal{M} and returns a parameter-dependent mapping $\Phi : \Omega \times \mathcal{P} \rightarrow \Omega$, which tracks coherent features (e.g., shocks, shear layers) of the solution field and ultimately simplifies the task of model reduction. We consider mappings of the form $\Phi = \mathbb{N}(\mathbf{a})$ where $\mathbb{N} : \mathbb{R}^M \rightarrow \text{Lip}(\Omega; \mathbb{R}^2)$ is a suitable linear or nonlinear operator; then, we state the registration problem as an unconstrained optimization statement for the coefficients \mathbf{a} . We identify minimal requirements for the operator \mathbb{N} to ensure the satisfaction of the bijectivity constraint; we propose a class of compositional maps that satisfy the desired requirements and enable non-trivial deformations over curved boundaries of Ω ; we develop a thorough analysis of the proposed ansatz for polytopal domains and we discuss the approximation properties for general curved domains. We perform numerical experiments for a parametric inviscid transonic compressible flow past a cascade of turbine blades to illustrate the many features of the method.

Keywords: parameterized partial differential equations; registration in bounded domains; model order reduction.

1 Introduction

1.1 Registration in bounded domains

Numerical methods based on Lagrangian (registration-based) approximations have proven to be a promising research direction in scientific computing, both for the numerical discretization of partial differential equations (PDEs) [24, 34] and also for model order reduction of parametric systems (MOR, [8, 15, 16, 23, 27]). Given the field of interest u defined over the domain $\Omega \subset \mathbb{R}^2$, Lagrangian methods seek approximations of the solution u of the form $\tilde{u} \circ \Phi^{-1}$ where \tilde{u} belongs to a linear approximation space and Φ is a mapping from Ω in itself. This class of methods is designed for problems with sharp features such as shocks, contact discontinuities or shear layers in fluid mechanics and fractures in solid mechanics. The problem of finding the mapping Φ is dubbed as registration problem and shares important features with geometry registration [14, 18] and mesh morphing [26, 31] techniques, and also optimal transportation [3, 10, 21]. The goal of this paper is to develop a general registration procedure for parametric problems with emphasis on parametric MOR applications, and to provide a rigorous mathematical analysis of the problem of registration in bounded two-dimensional domains.

We pursue an optimization-based approach to the problem of registration. We denote by μ a vector of P parameters in the parameter domain $\mathcal{P} \subset \mathbb{R}^P$; given the domain $\Omega \subset \mathbb{R}^2$, we denote by \mathfrak{B} the space of Lipschitz bijections from Ω in itself. Given the mapping Φ , we denote by $J(\Phi)$ the Jacobian determinant, and we denote by $\text{id} : \mathbb{R}^2 \rightarrow \mathbb{R}^2$ the identity map in \mathbb{R}^2 , $\text{id}(x) = x$ for all $x \in \mathbb{R}^2$. If we fix the value of $\mu \in \mathcal{P}$, we seek solutions to the problem

$$\min_{\Phi \in \mathcal{W}} f_\mu^{\text{obj}}(\Phi), \quad (1)$$

where \mathcal{W} is a finite-dimensional space of dimension M and $f^{\text{obj}} : \mathcal{W} \times \mathcal{P} \rightarrow \mathbb{R}_+$ is a suitable merit function. The problem of registration is uniquely characterized by the choice of the approximation space \mathcal{W} , the objective f^{obj} , and the numerical method to solve the resulting optimization problem. In view of the discussion, we introduce the operator $\mathbb{N} : \mathbb{R}^M \rightarrow \text{Lip}(\Omega; \mathbb{R}^2)$ that spans \mathcal{W} (that is, $\mathbb{N}(\mathbb{R}^M) = \mathcal{W}$), the set of admissible maps A , and the set of maps with positive Jacobian determinant A_{jac} :

$$A := \{\mathbf{a} \in \mathbb{R}^M : \mathbb{N}(\mathbf{a}) \in \mathfrak{B}\}, \quad A_{\text{jac}} := \{\mathbf{a} \in \mathbb{R}^M : \inf_{x \in \Omega} J(\mathbb{N}(\mathbf{a})) > 0\}. \quad (2)$$

In this paper, we focus on the choice of the approximation space \mathcal{W} or, equivalently, on the choice of the operator \mathbb{N} . Towards this end, we identify the following two requirements for \mathbb{N} :

1. the condition $\inf_{x \in \Omega} J(\Phi) > 0$ implies bijectivity in Ω for any $\Phi \in \mathcal{W}$, that is $A_{\text{jac}} \subset A$;

2. \mathbb{N} is Lipschitz-continuous with respect to the mapping coefficients \mathbf{a} .

The first requirement dramatically simplifies the enforcement of the bijectivity in Ω , since it suffices to construct an objective function $\mathfrak{f}^{\text{obj}}$ such that $\mathfrak{f}^{\text{obj}}(\Phi) > \mathfrak{f}^{\text{obj}}(\text{id})$ for any $\Phi \in \mathcal{W}$ for which $\inf_{x \in \Omega} J(\Phi) \leq 0$. Since the determinant is a differentiable function, the second requirement implies that A_{jac} is an open set in \mathbb{R}^M (cf. Corollary 2.4): provided that $A_{\text{jac}} \subset A$, we can thus apply gradient-based methods to solve (1) and ultimately deal with high-dimensional parameterizations (i.e., $M \gg 1$). It is possible to construct maps Φ that are bijective in Ω for which $\inf_{x \in \Omega} J(\Phi) = 0$ (cf. [22, Theorem 1.1]); however, we expect that bijections Φ which satisfy $\inf_{x \in \Omega} J(\Phi) = 0$ are of little practical interest for scientific computing applications and in particular for (projection-based) MOR.

We also require the additional condition:

3. $\mathbb{N}(\mathbf{a} = 0) = \text{id}$.

Thanks to this assumption, we find that $0 \in A_{\text{jac}} \subset A$; furthermore, given the full-rank matrix $\mathbf{W} \in \mathbb{R}^{M \times m}$ with $m \leq M$ we can easily verify that the operator $\tilde{\mathbb{N}}(\mathbf{a}) = \mathbb{N}(\mathbf{W}\mathbf{a})$ satisfies the three requirements introduced above. We can hence apply linear compression methods such as proper orthogonal decomposition (POD, [32]) to the mapping coefficients \mathbf{a} without fundamentally changing the properties of our ansatz. As discussed in sections 2 and 4, this feature greatly simplifies the task of dimensionality reduction for parametric problems.

1.2 Compositional maps for registration

In this work, we propose and analyze compositional maps of the form

$$\mathbb{N}(\mathbf{a}) = \Psi \circ \mathbb{N}_{\text{p}}(\mathbf{a}) \circ \Psi^{-1}, \quad (3)$$

where $\Psi : \Omega_{\text{p}} \rightarrow \Omega$ is a bijection from the polytope Ω_{p} to Ω and $\mathbb{N}_{\text{p}}(\mathbf{a}) : \Omega_{\text{p}} \rightarrow \Omega_{\text{p}}$ is affine in \mathbf{a} , that is $\mathbb{N}_{\text{p}}(\mathbf{a}) = \text{id} + \sum_{i=1}^M (\mathbf{a})_i \varphi_i$ for suitably chosen functions $\{\varphi_i\}_i$ whose normal components vanish on $\partial\Omega_{\text{p}}$, $\varphi_i \cdot \mathbf{n}|_{\partial\Omega_{\text{p}}} = 0$ for $i = 1, \dots, M$. We also discuss the multi-layer generalization of (3)

$$\mathbb{N}(\mathbf{a} = [\mathbf{a}_1, \dots, \mathbf{a}_\ell]) = \mathbb{N}_1(\mathbf{a}_1) \circ \dots \circ \mathbb{N}_\ell(\mathbf{a}_\ell), \quad (4)$$

where $\mathbb{N}_i(\mathbf{a}_i) = \Psi_i \circ \mathbb{N}_{\text{p},i}(\mathbf{a}_i) \circ \Psi_i^{-1}$ with $\Psi_i : \Omega_{\text{p},i} \rightarrow \Omega_i$ is a Lipschitz bijection and $\Omega_{\text{p},i}$ is a suitable polytope, for $i = 1, \dots, \ell$.

We provide a complete analysis of affine maps in polytopes. First, we show that affine maps satisfy the three requirements introduced above (cf. Proposition 2.1 and Corollary 2.3); we also show that affine maps are dense for $M \rightarrow \infty$ in a meaningful subspace of C^1 bijections (cf. Proposition 2.2 and Corollary 2.5).

We exploit the analysis of registration in polytopes to study the properties of maps of the form (3) and (4) in arbitrary domains. First, we prove that affine maps are fundamentally ill-suited to approximate non-trivial diffeomorphisms in curved domains; second, we discuss the approximation properties of the maps (3) and then of the maps (4). Finally, we propose an actionable strategy to define the polytope Ω_{p} and the mapping Ψ : our approach relies on the definition of a coarse-grained curved high-order finite element (FE) mesh \mathcal{T}_{hf} of Ω , and to a fully-automated procedure to define the polytope Ω_{p} and the map Ψ based on the curved mesh \mathcal{T}_{hf} .

Our method is related to several previous works. A first extension of the registration procedure in [27] to arbitrary domains was proposed in [29]: the work of [29] relies on the introduction of a coarse-grained partition of the domain Ω and on Gordon-Hall maps to morph each element of the partition into the unit square. The approach in [29] requires that each element of the partition is mapped in itself (*local bijectivity*) and relies on Gordon-Hall maps: it is hence very sensitive to the choice of the coarse-grained partition, it is not dense in any meaningful subset of diffeomorphisms, and it cannot be extended to three-dimensional domains. We also recall the work by Zahr and Persson [35] for high-order implicit shock tracking methods: the approach in [35] relies on a local parameterization of boundary degrees of freedom; for this reason, it cannot be readily combined with linear dimensionality reduction techniques to identify low-rank mapping spaces for parametric systems. We finally remark that the multi-layer ansatz (4) is closely related to registration methods appeared in the image processing literature [5, 6].

We here rely on a standard H^1 -conforming FE discretization to represent the mapping; on the other hand, as in our previous works (e.g., [27, 29]), we aim to include an H^2 penalization term in the objective $\mathfrak{f}^{\text{obj}}$. Towards this end, we propose a discrete H^2 broken norm that is inspired by the work by Mozolevski and coauthors [17] on discontinuous Galerkin (DG) discretizations of the biharmonic equation. Following the seminal work by Argyris and coauthors [1], several researchers have considered H^2 -conforming FE spaces for the discretization of fourth-order operators: the use of standard FE discretizations simplifies the implementation and also enables the application of polynomial bases of arbitrary order.

The outline of the paper is as follows. Section 2 provides a complete analysis of registration in polytopes; section 3 addresses the extension to curved domains; section 4 discusses the construction of the polytope

Ω_p and the mapping Ψ and reviews the parametric registration method proposed in [29] and employed in the numerical experiments; section 5 contains numerical investigations to illustrate the performance of the registration method and its implications for model reduction. We here couple our registration procedure with a non-intrusive (POD+regression) MOR procedure for state estimation; the integration of registration in the offline-online computational paradigm of projection-based MOR is the subject of ongoing research. Section 6 concludes the paper.

2 Affine maps in polytopes

In section 2.1, we present two technical results for affine maps in polytopes; in sections 2.2 and 2.3, we illustrate the implications of these results to the problem of registration in polytopal domains; finally, in section 2.4 we comment on the approximation of Lipschitz maps.

2.1 Mathematical background

We say that $\Omega_p \subset \mathbb{R}^2$ is a polytope if the boundary of Ω_p , $\partial\Omega_p$, consists of a finite number of flat sides (*faces*). The boundary of two-dimensional polytopes is described by a finite number of straight segments (*edges*) connected to form (possibly several disjoint) closed polygonal chains; the points of $\partial\Omega_p$ where two consecutive edges meet are dubbed *vertices*; the union of all vertices is here denoted by $V = \{x_i^v\}_{i=1}^{N_v}$. We here consider polytopes that satisfy the condition below (cf. Figure 1).

Definition 2.1. *The polytope Ω_p is said to be regular if each vertex x^v is the intersection of two edges.*

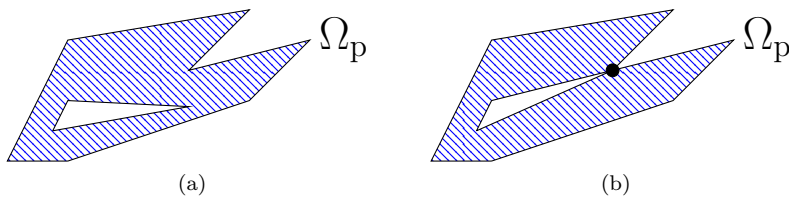


Figure 1: interpretation of definition 2.1. (a) regular polytope. (b) irregular polytope.

We denote by $\mathbf{n}(x)$ the outward normal to Ω_p at $x \in \partial\Omega_p$; we also denote by $\bar{\Omega}_p$ the closure of Ω_p in \mathbb{R}^2 . Given the vector-valued function $\Phi : \Omega_p \rightarrow \mathbb{R}^2$, we denote by $J(\Phi) = \det(\nabla\Phi)$ the Jacobian determinant and we recall the definition of the identity map $\text{id} : \mathbb{R}^2 \rightarrow \mathbb{R}^2$ such that $\text{id}(x) = x$ for all $x \in \mathbb{R}^2$. Propositions 2.1 and 2.2 contain two important results for mappings in polytopes. The proof of Proposition 2.1 is technical and is postponed to Appendix A.

Proposition 2.1. *Let Ω_p be a regular bounded polytope. Define the space $\mathfrak{U}_p = \{\varphi \in C^1(\bar{\Omega}_p; \mathbb{R}^2) : \varphi \cdot \mathbf{n}|_{\partial\Omega_p} = 0\}$ and consider the vector-valued function $\Phi = \text{id} + \varphi$ with $\varphi \in \mathfrak{U}_p$. Then, Φ is a bijection in Ω_p if $\min_{x \in \bar{\Omega}_p} J(\Phi) > 0$.*

Proposition 2.2. *Let Φ be a C^1 mapping from Ω_p in itself. Then, $\Phi(V) = V$. Furthermore, if $\Phi(x^v) = x^v$ for all $x^v \in V$, then $\Phi = \text{id} + \varphi$ with $\varphi \in \mathfrak{U}_p$.*

Proof. Let $x^v \in V$ and define $y = \Phi(x^v)$; recalling Nanson's formula, we find that the normal to $\Phi(\Omega_p)$ satisfies $\mathbf{n}_\Phi(y) \propto J(\Phi(x))(\nabla\Phi(x))^{-T}\mathbf{n}(x)$; therefore, if $x \in \partial\Omega_p \mapsto \mathbf{n}(x)$ is discontinuous at x^v , we must have that $x \mapsto \mathbf{n}_\Phi(x)$ is discontinuous at y . Recalling the definition of vertices, we conclude that $y \in V$ for any $x^v \in V$, that is $\Phi(V) \subset V$. Since Φ is a bijection in Ω_p , the image points $\{\Phi(x^v) : x^v \in V\}$ should all be distinct and thus $\text{card}(\Phi(V)) = \text{card}(V)$, which implies $\Phi(V) = V$.

Let Φ satisfy the condition $\Phi(x^v) = x^v$ for all $x^v \in V$ and define the displacement $\varphi = \Phi - \text{id}$. Consider the edge $F \subset \partial\Omega_p$ and consider the parameterization $\gamma_f : [0, 1] \rightarrow F$ such that $\gamma_f(s) = x_1^v + s\|x_2^v - x_1^v\|_2\mathbf{t}_f$. Since $\partial\Omega_p$ is closed and $\Phi(\partial\Omega_p) = \partial\Omega_p$, we either have $\Phi(F) = \partial\Omega_p \setminus F$ or $\Phi(F) = F$. Recalling the expression for the normal \mathbf{n}_Φ , we find that \mathbf{n}_Φ is continuous in $\Phi(F)$: since $\partial\Omega_p \setminus F$ contains at least one vertex in addition to x_1^v, x_2^v (we here exploit the fact that two-dimensional polytopes have at least three vertices), we must have $\Phi(F) = F$.

The condition $\Phi(F) = F$ implies that $\Phi(\gamma_f(s)) = x_1^v + \alpha(s)\mathbf{t}_f$ for all $s \in [0, 1]$ and for some injective function $\alpha : [0, 1] \rightarrow [0, \|x_2^v - x_1^v\|_2]$. Given $x \in F$, since $\mathbf{n}(x) = \mathbf{n}_f$ and $\mathbf{n}_f \perp \mathbf{t}_f$, we find

$$\mathbf{n}(x) \cdot \varphi(x) = \mathbf{n}_f \cdot (\Phi(x) - x) = \mathbf{n}_f \cdot (x_1^v + \alpha(s)\mathbf{t}_f - x_1^v - s\|x_2^v - x_1^v\|_2\mathbf{t}_f) = 0,$$

which is the desired result. \square

2.2 Construction of finite-dimensional operators for registration

We introduce the finite-dimensional space \mathcal{U}_p spanned by $\{\varphi_i\}_{i=1}^M \subset \mathfrak{U}_p$, and the affine space $\mathcal{W}_p := \text{id} + \mathcal{U}_p$. We introduce the operator $N_p : \mathbb{R}^M \rightarrow \mathcal{W}_p$ such that $N_p(\mathbf{a}) = \text{id} + \sum_{i=1}^M \mathbf{a}_i \varphi_i$. Exploiting Proposition 2.1, we can show that the operator N_p satisfies the three requirements stated in the introduction for the polytope Ω_p . The proof is straightforward and is here omitted. For completeness, we also show that the interior of the admissible set A (2) is not empty.

Corollary 2.3. *Let $\mathcal{U}_p = \text{span}\{\varphi_i\}_{i=1}^M$ be an M -dimensional subspace of \mathfrak{U}_p . Then, the affine operator N_p satisfies the following properties: (i) the condition $\inf_{x \in \Omega_p} J(N_p(\mathbf{a})) > 0$ implies bijectivity in Ω_p ; (ii) N_p is differentiable with respect to the mapping coefficients; and (iii) $N_p(0) = \text{id}$.*

Corollary 2.4. *Let $\Phi = \text{id} + \varphi$ with $\varphi \in \mathfrak{U}_p$ satisfy $\min_{x \in \overline{\Omega_p}} J(\Phi) > 0$. Then, there exists $r > 0$ such that for any $\psi \in \mathfrak{U}_p$ such that $\|\nabla\psi - \nabla\varphi\|_{L^\infty(\Omega_p)} < r$, the function $\Psi = \text{id} + \psi$ is also a bijection from Ω_p in itself.*

Proof. Since the determinant is a continuous matrix-valued function, there exists $C > 0$ such that $\|J(\text{id} + \psi) - J(\Phi)\|_{L^\infty(\Omega_p)} \leq C\|\nabla\psi - \nabla\varphi\|_{L^\infty(\Omega_p)}$ for any $\psi \in \mathfrak{U}_p$. Therefore, if we define $\epsilon = \min_{x \in \overline{\Omega_p}} J(\Phi)$, the mapping $\Psi = \text{id} + \psi$ satisfies the condition $\min_{x \in \overline{\Omega_p}} J(\Psi) > 0$ for any ψ such that $\|\nabla\psi - \nabla\varphi\|_{L^\infty(\Omega_p)} < \frac{\epsilon}{C} =: r$. Exploiting Proposition 2.1, we conclude that Ψ is a bijection from Ω_p in itself for any ψ such that $\|\nabla\psi - \nabla\varphi\|_{L^\infty(\Omega_p)} < r$. \square

2.3 Approximation properties of affine mappings

Proposition 2.2 shows that bijections are of the form $\Phi = \text{id} + \varphi$ with $\varphi \in \mathfrak{U}_p$ if and only if $\Phi(x^v) = x^v$ for all $x^v \in V$. It is easy to construct bijections that do not fulfill this requirement: to provide a concrete example, consider the map $\Phi(x) = -x$ for the polytope $\Omega_p = (-1, 1)^2$. However, in the setting of MOR and also geometry reduction, we are interested in parametric maps that are smooth deformations of the identity map: since registration is applied with respect to an element of the solution manifold $\mathcal{M} = \{u_\mu : \mu \in \mathcal{P}\}$, we can indeed assume that there exists $\mu \in \mathcal{P}$ such that $\Phi_\mu = \text{id}$. We hence have the following result, which follows from Proposition 2.2.

Corollary 2.5. *Let $\Phi : \Omega_p \times \mathcal{P} \rightarrow \Omega_p$ be a continuous function of the parameter $\mu \in \mathcal{P}$ and let Φ_μ be a C^1 map (diffeomorphism) for all $\mu \in \mathcal{P}$, and that \mathcal{P} is simply connected. Assume that $\Phi_{\mu'} = \text{id}$ for some $\mu' \in \mathcal{P}$. Then, $\Phi_\mu = \text{id} + \varphi_\mu$ with $\varphi_\mu \in \mathfrak{U}_p$ for all $\mu \in \mathcal{P}$.*

Proof. Since the set of vertices V is a discrete closed set, if the function $\Phi : \Omega_p \times \mathcal{P} \rightarrow \Omega_p$ is continuous with respect to the parameter $\mu \in \mathcal{P}$ and is bijective from Ω_p in itself for all $\mu \in \mathcal{P}$, then the condition $\Phi_{\mu'}|_V = \text{id}$ for some $\mu' \in \mathcal{P}$ implies $\Phi_\mu|_V = \text{id}$ for all $\mu \in \mathcal{P}$. Therefore, exploiting the second statement of Proposition 2.2, we conclude that $\Phi_\mu = \text{id} + \varphi_\mu$ with $\varphi_\mu \in \mathfrak{U}_p$ for all $\mu \in \mathcal{P}$. \square

Given the parametric registration problem (1) with $\mathcal{W}_p = \text{id} + \mathfrak{U}_p$, we denote by $\Phi_\mu^{\text{opt}} = \text{id} + \varphi_\mu^{\text{opt}}$ a solution to (1) for any $\mu \in \mathcal{P}$ and we define corresponding manifold $\mathcal{M}_\Phi := \{\varphi_\mu^{\text{opt}} : \mu \in \mathcal{P}\} \subset \mathfrak{U}_p$. If \mathcal{M}_Φ is reducible — that is, there exists a low-dimensional space $\mathcal{U}_p = \text{span}\{\varphi_i\}_{i=1}^m$ with $m = \mathcal{O}(1-10)$ that accurately approximates all elements of \mathcal{M}_Φ — we can restrict the search space in (1) to $\mathcal{W}_p = \text{id} + \mathcal{U}_p$. Note that, since the operator N_p associated to \mathcal{U}_p satisfies the hypotheses of Corollary 2.3 for any choice of \mathcal{U}_p , the choice of the approximation space can be made solely based on approximation considerations.

2.4 Approximation of Lipschitz maps

The proof of Proposition 2.1 exploits the Hadamard's global inverse function theorem (cf. [12, Theorem 6.2.8]); it hence relies on the assumption that Φ is of class C^1 . Our numerical investigations suggest that a similar result — possibly with further conditions — might hold for piecewise-smooth maps such as FE fields.

On the other hand, Proposition 2.2 does not hold for general Lipschitz maps, as shown in the next example. First, we introduce the square domain $\Omega = (0, 1)^2$, and we define the map $\Phi_1 : \Omega = (0, 1)^2 \rightarrow \mathbb{R}^2$ such that

$$\Phi_1(x) = \begin{bmatrix} 1/2 & 0 \\ -1/2 & 1 \end{bmatrix} x \mathbb{1}_{x_1 < x_2}(x) + \begin{bmatrix} 1 & -1/2 \\ 0 & 1/2 \end{bmatrix} x \mathbb{1}_{x_1 \geq x_2}(x). \quad (5)$$

It is easy to verify that Φ_1 is a Lipschitz map from Ω in the unit triangle $D = \{x \in \Omega : x_1 + x_2 < 1\}$ with Lipschitz inverse (cf. Figure 2(a)). Then, we introduce a smooth bijection $\Phi_2 : D \rightarrow D$ that maps $x^* = [1/2, 1/2]$ into $y^* = [1/4, 3/4]$ (cf. Figure 2(b)): Φ_2 can be constructed using an expansion of quadratic polynomials; we omit the explicit expression. Finally, we define the map $\Phi = \Phi_1^{-1} \circ \Phi_2 \circ \Phi_1$: clearly, Φ is a bijection from Ω in itself; furthermore, $\Phi([1, 1]) = \Phi_1^{-1}(\Phi_2([1/2, 1/2])) = \Phi_1^{-1}([1/4, 3/4]) = [1, 1/2]$. We hence found a bijection Φ in Ω such that $\Phi(V) \neq V$.

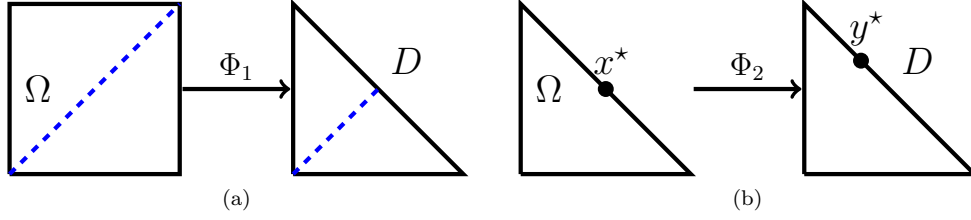


Figure 2: example of Lipschitz map with $\Phi(V) \neq V$. (a) Lipschitz map from the unit square to the unit triangle (cf (5)). (b) smooth map in the unit triangle D .

3 Nonlinear maps for general domains

We address the extension to non-polytopal domains. First, we justify the need for nonlinear ansatz; then, we investigate the approximation properties of the nonlinear ansatz (3) and (4).

3.1 Inadequacy of affine maps for domains with curved boundaries

It is trivial to extend Proposition 2.1 to an arbitrary domain Ω by replacing the space $\mathfrak{U} = \{\varphi \in C^1(\bar{\Omega}; \mathbb{R}^2) : \varphi \cdot \mathbf{n}|_{\partial\Omega} = 0\}$ with the space $\mathfrak{U}_0 = \{\varphi \in C^1 : \varphi = 0\}$: we have indeed that any function $\Phi = \text{id} + \varphi$ with $\varphi \in \mathfrak{U}_0$ satisfies $\Phi(\partial\Omega) = \partial\Omega$; we can thus directly apply [27, Proposition 2.1] (see also Proposition A.1). However, this choice of the search space prevents us from deforming points that lie on curved edges or faces.

Next result, which generalizes [29, Lemma 2.1], shows that non-trivial affine mappings for curved domains lead to admissible sets A with empty interior: affine maps hence violate the first requirement stated in the introduction. This observation shows the inadequacy of affine maps for domains with curved boundaries and ultimately justifies the need for a nonlinear ansatz.

Lemma 3.1. *Let $\Omega \subset \mathbb{R}^2$ be a domain with curved boundary $\Gamma \subset \partial\Omega$; let $N : \mathbb{R}^M \rightarrow \text{Lip}(\bar{\Omega}; \mathbb{R}^2)$ be an affine operator of the form $N(\mathbf{a}) = \text{id} + \sum_{i=1}^M (\mathbf{a})_i \varphi_i$ and let $A \subset \mathbb{R}^M$ be the set of admissible (i.e., bijective in Ω) maps. Suppose that there exists $i \in \{1, \dots, M\}$ and $x \in \Gamma$ such that $\varphi_i(x) \neq 0$. Then, $0 \in \mathbb{R}^M$ does not belong to the interior of A . Furthermore, if $\Gamma = \partial\Omega$, then A has empty interior.*

Proof. By contradiction, there exists $r > 0$ such that $\mathcal{B}_r(0) \subset A$; therefore, there exists $\delta > 0$ such that $\Phi_t = \text{id} + t\varphi_i$ is a bijection in Ω for all $t \in (-\delta, \delta)$. Since Φ_t is bijective in Ω , we must have $\Phi_t(\partial\Omega) = \partial\Omega$, which implies that the linear segment $S_\delta = \{x + t\varphi_i(x) : t \in (-\delta, \delta)\}$ is contained in $\partial\Omega$. We conclude that $\partial\Omega$ is flat in the neighborhood of $x \in \Gamma$. Contradiction.

We remark that the argument of the proof solely relies on the fact that $\Phi_{t=0}(x) \in \Gamma$: if $\partial\Omega$ is entirely curved (that is, if $\Gamma = \partial\Omega$) we can replicate the same argument for any $\mathbf{a} \in A$ to prove that A has empty interior. \square

3.2 Approximation properties of compositional maps

Given the compositional maps (3), we denote by $V = \{x_i^v\}_{i=1}^{N_v}$ the vertices of Ω_p and we denote by $\{F_j^p\}_{j=1}^{N_f}$ the facets of Ω_p ; we also define the mapped vertices $W = \{y_i^v = \Psi(x_i^v)\}_{i=1}^{N_v}$ and the mapped facets $\{F_j = \Psi(F_j^p)\}_{j=1}^{N_f}$. By construction, we find that mappings Φ of the form (3) satisfy $\Phi|_W = \text{id}$ and $\Phi(F_j) = F_j$ for $j = 1, \dots, N_f$. Conversely, we have the following result, which signifies that nonlinear maps of the form (3) are dense in the space of diffeomorphisms that satisfy $\Phi|_W = \text{id}$.

Lemma 3.2. *Let Φ be a C^1 bijection from Ω in itself such that $\Phi|_W = \text{id}$. Then, $\tilde{\Phi} = \Psi^{-1} \circ \Phi \circ \Psi = \text{id} + \varphi$ for some $\varphi \in \text{Lip}(\Omega_p; \mathbb{R}^2)$ such that $\varphi \cdot \mathbf{n}|_{\partial\Omega_p} = 0$.*

Proof. Since $\Phi|_W = \text{id}$ and Φ is a diffeomorphism, we must have $\Phi(F_j) = F_j$ for $j = 1, \dots, N_f$; therefore, we have that $\tilde{\Phi}$ is a bijection in Ω_p that satisfies $\tilde{\Phi}(F_j^p) = F_j^p$ for $j = 1, \dots, N_f$. Then, exploiting the same argument of the proof of Proposition 2.2, we find that $\tilde{\Phi} = \text{id} + \varphi$ with $\varphi \cdot \mathbf{n}|_{\partial\Omega_p} = 0$. We omit the details. \square

3.3 Multi-layer compositional maps

Lemma 3.2 shows that single-layer compositional maps cannot approximate arbitrary diffeomorphisms in curved domains. To address this issue, we might consider more general multi-layer maps of the form (4). We here study the approximation properties of (4) for $\ell = 2$ layers

$$N(\mathbf{a}_1, \mathbf{a}_2) = N_1(\mathbf{a}_1) \circ N_2(\mathbf{a}_2), \quad N_i(\mathbf{a}_i) = \Psi_i \circ N_{p,i}(\mathbf{a}_i) \circ \Psi_i^{-1}, \quad i = 1, 2.$$

We denote by $\Omega_{p,1}$ and $\Omega_{p,2}$ the polytopes associated to the bijections Ψ_1, Ψ_2 . We also denote by $V_i^{\text{fict}} = \{x_{j,i}^v\}_{j=1}^{N_{v,i}}$ the *fictitious* vertices of $\Omega_{p,i}$, that is, the vertices of $\Omega_{p,i}$ that do not correspond to angular points of Ω . Finally, given $x, y \in \partial\Omega$, we define the set of curves

$$A_{\partial\Omega}(x, y) = \{ \gamma \in C^1([0, 1]; \partial\Omega) : \gamma(0) = x, \gamma(1) = y, \|\dot{\gamma}\|_2 \equiv \text{const} \} \quad (6a)$$

and the geodesic distance

$$\text{dist}_{\partial\Omega}(x, y) = \begin{cases} \inf \left\{ \int_0^1 \|\dot{\gamma}\|_2 dt : \gamma \in A_{\partial\Omega}(x, y) \right\} & \text{if } A_{\partial\Omega}(x, y) \neq \emptyset \\ +\infty & \text{if } A_{\partial\Omega}(x, y) = \emptyset \end{cases} \quad (6b)$$

Next Lemma shows that two-layer maps can approximate arbitrary diffeomorphisms under the assumption of small deformations.

Lemma 3.3. *Let Φ be a diffeomorphism from Ω in itself such that $\max_{x \in \partial\Omega} \text{dist}_{\partial\Omega}(x, \Phi(x)) < C$ where $C = C(\Omega_{p,1}, \Omega_{p,2})$ is given by*

$$C := \min_{x \in V_1^{\text{fict}}, y \in V_2^{\text{fict}}} \text{dist}_{\partial\Omega}(\Psi_1(x), \Psi_2(y)). \quad (7)$$

Then, there exist $\Phi_1 = \text{id} + \varphi_1$ and $\Phi_2 = \text{id} + \varphi_2$ such that $\Phi = \Psi_1 \circ \Phi_1 \circ \Psi_1^{-1} \circ \Psi_2 \circ \Phi_2 \circ \Psi_2^{-1}$ and $\varphi_i \cdot \mathbf{n}|_{\partial\Omega_{p,i}} = 0$ for $i = 1, 2$.

Proof. We denote by $z_j = \Phi(x_{j,2}^v)$ the mapped vertices for $j = 1, \dots, N_{v,2}$. For any $j = 1, \dots, N_{v,2}$, since $\text{dist}_{\partial\Omega}(z_j, x_{j,2}^v) < C$, there exists a facet $F_{k_j}^{p,1}$ of $\Omega_{p,1}$ that contains both z_j and $x_{j,2}^v$: therefore, there exists a map $\tilde{\Phi} = \Psi_1 \circ \Phi_1 \circ \Psi_1^{-1}$ with $\Phi_1 = \text{id} + \varphi_1$ and $\varphi_1 \cdot \mathbf{n}|_{\partial\Omega_{p,1}} = 0$ such that $\tilde{\Phi}(x_{j,2}^v) = z_j$ for $j = 1, \dots, N_{v,2}$.

We now consider the map $\tilde{\Phi}^{-1} \circ \Phi$: clearly, the map is Lipschitz and satisfies $\tilde{\Phi}^{-1} \circ \Phi(x_{j,2}^v) = x_{j,2}^v$ for $j = 1, \dots, N_{v,2}$. We can thus apply Lemma 3.2 to prove the existence of a map $\Phi_2 = \text{id} + \varphi_2$ with $\varphi_2 \cdot \mathbf{n}|_{\partial\Omega_{p,2}} = 0$ such that $\tilde{\Phi}^{-1} \circ \Phi = \Psi_2 \circ \Phi_2 \circ \Psi_2^{-1}$, which is the desired result. \square

The extension to multiple layers enables the approximation of diffeomorphisms that involve larger deformations over curved edges. Figure 3 illustrates the approximation power of multi-layer maps for deformations over an airfoil: Figure 3(a) shows the two polytopes $\Omega_{p,1}, \Omega_{p,2}$ that are used to define the nonlinear ansatz and two points x, y on the profile such that $\Phi(x) = y$; Figures 3(b)-(c)-(d) show the action of the maps N_3, N_2 and N_1 , respectively. In more detail, the map N_3 — which is associated to $\Omega_{p,1}$ — deforms the point x in the point x_1 (cf. Figure 3(b)); the map N_2 — which is associated to $\Omega_{p,2}$ — deforms the point x_1 in the point x_2 (cf. Figure 3(c)); the map N_1 — which is associated to $\Omega_{p,1}$ — deforms the point x_2 in the point y (cf. Figure 3(d)). In conclusion, the considered map satisfies $N_1(N_2(N_3(x))) = y$.

3.4 Discussion

The analysis of this section shows that compositional maps (3) and their multi-layer generalization (4) can be employed for registration in curved domains. Since Ψ in (3) and Ψ_1, \dots, Ψ_ℓ in (4) are independent of the coefficients \mathbf{a} , we can exploit Proposition 2.1 (see also the discussion in section 2.2) to prove that (3) and (4) satisfy the three requirements listed in the introduction.

Lemmas 3.2 and 3.3 investigate the approximation properties of the ansatzs (3) and (4): the analysis shows that multi-layer maps provide much more approximation power, even for moderate number of layers ℓ . We note, however, that multi-layer maps are considerably more challenging to implement and might also be significantly more expensive to evaluate: the solution to (1) requires indeed many evaluations of the mapping $\mathbf{N}(\mathbf{a})$ and its gradient, which involve the evaluation of the bijections $\{\Psi_i\}_{i=1}^\ell$ and their inverses. In this work, we focus on the implementation of registration strategies based on the more elementary ansatz (3) and we refer to a future work for the implementation of registration methods based on the model class (4).

4 Methodology

Given the domain $\Omega \subset \mathbb{R}^2$, we present a registration procedure based on compositional mappings of the form (3). In section 4.1, we introduce a finite element (FE) space \mathcal{U}_p for the displacement field in the polytope Ω_p and we discuss the choice of the functional norm $\|\cdot\|$ for \mathcal{U}_p ; then, in section 4.2, we discuss the construction of the polytope Ω_p and of the mapping Ψ in (3). In sections 4.3 and 4.4, we review the formulation of the optimization problem proposed in [27, 29] and the extension to parametric problems. To simplify the presentation, we here assume that the domain Ω is parameter-independent.

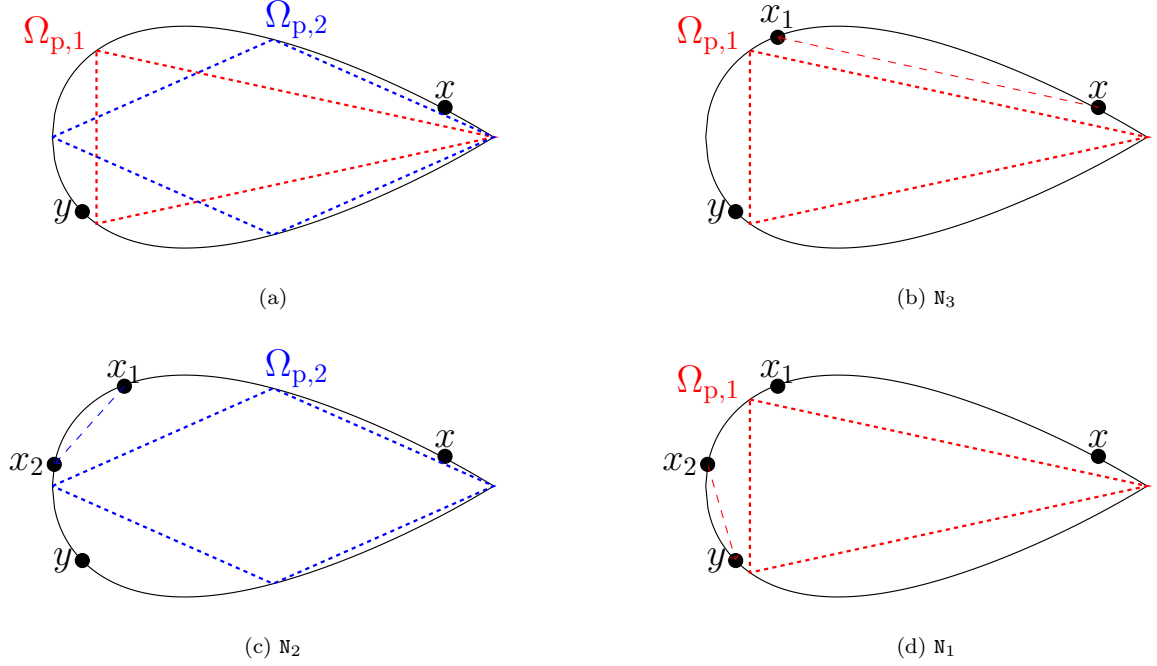


Figure 3: approximation of large deformations over curved boundaries using a multi-layer ($\ell = 3$) compositional map.

4.1 Finite element displacement space on polytopes

Given the polytope $\Omega_p \subset \mathbb{R}^2$, we define the linear mesh $\mathcal{T}_p = \{\mathcal{D}_{k,p}\}_{k=1}^{N_e}$ where $\mathcal{D}_{k,p}$ is the k -th element of the mesh. We define the reference (or master) element $\widehat{\mathcal{D}} = \{x \in (0,1)^2 : \sum_{i=1}^2 (x)_i < 1\}$ and the linear maps $\{\Psi_{k,p}\}_k$ that map $\widehat{\mathcal{D}}$ into the elements of the mesh. Then, we introduce the space \mathcal{U}_p for the displacement field (cf. section 2):

$$\mathcal{U}_p = \left\{ \varphi \in [\mathcal{X}_{\text{hf},p}]^2 : \varphi \cdot \mathbf{n}|_{\partial\Omega_p} = 0 \right\}, \quad \text{with } \mathcal{X}_{\text{hf},p} = \left\{ \phi \in C(\Omega_p) : \phi|_{\mathcal{D}_{k,p}} \in \mathbb{P}_\kappa \right\} \quad (8)$$

and \mathbb{P}_κ denotes the space of polynomials of degree at most $\kappa > 0$. We further define the facets $\{\mathcal{F}_{j,p}\}_{j=1}^{N_f}$ of \mathcal{T}_p with positive¹ normal \mathbf{n}^+ and we denote by $\mathcal{I}_{\text{int}} \subset \{1, \dots, N_f\}$ the indices of the internal facets. We denote by $\mathcal{E}_p^{\text{int}} = \bigcup_{j \in \mathcal{I}_{\text{int}}} \mathcal{F}_{j,p}$ the union of internal facets. Given the field $\phi \in \mathcal{X}_{\text{hf},p}$ and the differential operator \mathfrak{L} , we define the limits

$$\mathfrak{L}(\phi)^\pm(x) = \lim_{\epsilon \rightarrow 0^+} \mathfrak{L}(\phi)(x \mp \epsilon \mathbf{n}^+(x)), \quad \forall x \in \mathcal{E}_p^{\text{int}}, \quad (9a)$$

and the average and jump operators (we omit dependence on x)

$$\{\mathfrak{L}(\phi)\} = \frac{\mathfrak{L}(\phi)^+ + \mathfrak{L}(\phi)^-}{2}, \quad \llbracket \mathfrak{L}(\phi) \rrbracket = (\mathfrak{L}(\phi)^+ - \mathfrak{L}(\phi)^-) \cdot \mathbf{n}^+, \quad (9b)$$

for all $x \in \mathcal{E}_p^{\text{int}}$. We clarify that if $\mathfrak{L}(\phi)$ is a matrix-valued quantity the jump operator involves a matrix-vector product.

We observe that \mathcal{U}_p (8) is contained in the space of Lipschitz functions in Ω_p but it is not contained in $C^1(\Omega_p)$. In order to control the jump of the mapping derivatives across elements, we equip \mathcal{U}_p with the inner product

$$(w, v) = \sum_{k=1}^{N_e} \int_{\mathcal{D}_{k,p}} (H(w) : H(v) + w \cdot v) dx + \sum_{j \in \mathcal{I}_{\text{int}}} \int_{\mathcal{F}_{j,p}} \left(\beta_j \llbracket \nabla w \rrbracket \cdot \llbracket \nabla v \rrbracket + \frac{1}{\beta_j} \{H(w)\} : \{H(v)\} \right) dx, \quad (10)$$

where $H(w) \in \mathbb{R}^{d \times d \times d}$ is the Hessian of w , $H(w) : H(v) = \sum_{i,j,k=1}^2 \partial_{i,j} w_k \partial_{i,j} v_k$, and $\beta_j = \sigma_\beta \kappa^2 |\mathcal{F}_{j,p}|^{-1}$ with $\sigma_\beta = 10$ and $j \in \mathcal{I}_{\text{int}}$; we further define the induced norm $\|\cdot\| = \sqrt{(\cdot, \cdot)}$. The choice of the inner product is

¹The positive normal is chosen arbitrarily for internal facets and coincides with the outward normal to Ω_p for boundary facets.

inspired by the analysis in [17, section 4] for the biharmonic equation: the authors of [17] consider the norm

$$\begin{aligned} \|w\|^2 &= \sum_{k=1}^{N_e} \|\Delta w\|_{L^2(\mathbb{D}_{k,p})}^2 + \sum_{j \in \mathbb{I}_{\text{int}}} \|\sqrt{\alpha} \llbracket w \rrbracket\|_{L^2(\mathbb{F}_{j,p})}^2 \\ &+ \|\sqrt{\beta} \llbracket \nabla w \rrbracket\|_{L^2(\mathbb{F}_{j,p})}^2 + \|1/\sqrt{\beta} \{\Delta w\}\|_{L^2(\mathbb{F}_{j,p})}^2 + \|1/\sqrt{\alpha} \{\nabla \Delta w\}\|_{L^2(\mathbb{F}_{j,p})}^2, \end{aligned}$$

for proper choices of α and β . Since we here consider continuous discretizations, we omit in (10) the first and fourth terms in the facet integral and we consider the same expression for β as in [17]; furthermore, since we wish to consider the full H^2 norm, we replace Δw with $H(w)$ in the volumetric and surface integral.

We here rely on polynomial discretizations of very high-order (up to $\kappa = 10$): to ensure accurate and stable computations, we rely on a nodal-based discretization that exploits Koornwinder polynomials to represent the local shape functions and to a tensor product of Gauss and Gauss–Radau quadratures (see, e.g., [7, 11]).

In view of the definition of the objective function in (1) in section 4.3, we also define the seminorm

$$\begin{aligned} \mathfrak{P}(\varphi) &= \sum_{k=1}^{N_e} \int_{\mathbb{D}_{k,p}} (H(\varphi) : H(\varphi)) \, dx \\ &+ \sum_{j \in \mathbb{I}_{\text{int}}} \int_{\mathbb{F}_{j,p}} \left(\beta_j \llbracket \nabla \varphi \rrbracket \cdot \llbracket \nabla \varphi \rrbracket + \frac{1}{\beta_j} \{H(\varphi)\} : \{H(\varphi)\} \right) \, dx. \end{aligned} \quad (11)$$

Note that $\mathfrak{P}(\Phi) = 0$ for any linear map $\Phi = \mathbf{b} + \mathbf{A}x$; in particular, $\mathfrak{P}(\text{id}) = 0$. We also define the penalty

$$\mathfrak{P}_{\text{brkn}}(\varphi) = \sum_{k=1}^{N_e} \int_{\mathbb{D}_{k,p}} (H(\varphi) : H(\varphi)) \, dx, \quad (12)$$

which does not penalize discontinuities of the displacement derivative at elements' interfaces.

4.2 Construction of the Lipschitz map Ψ on a coarse-grained mesh

Given the domain Ω , we introduce a coarse curved mesh $\mathcal{T} = \{\mathbb{D}_k\}_{k=1}^{N_e}$ of degree $\kappa > 0$. We define the reference vertices and nodes $\{\tilde{x}_i^{\mathbb{P}}\}_{i=1}^{d+1} \subset \{\tilde{x}_i\}_{i=1}^{n_{\text{lp}}} \subset \widehat{\mathbb{D}}$ and the associated Lagrangian bases $\{\ell_i^{\text{fe,p}}\}_{i=1}^{d+1}$ of \mathbb{P}_1 and $\{\ell_i^{\text{fe}}\}_{i=1}^{n_{\text{lp}}}$ of \mathbb{P}_κ . Then, for each element \mathbb{D}_k of the mesh, we define the nodes $\{x_{i,k}^{\text{hf}}\}_{i,k}$ such that $x_{i,k}^{\text{hf}}$ is the i -th node of the k -th element of the mesh \mathcal{T} for $i = 1, \dots, n_{\text{lp}}$ and $k = 1, \dots, N_e$; similarly, we define the vertices $\{x_{j,k}^{\text{hf,v}}\}_{j,k}$. Finally, we introduce the FE mappings

$$\Psi_k(\tilde{x}) = \sum_{i=1}^{n_{\text{lp}}} x_{i,k}^{\text{hf}} \ell_i^{\text{fe}}(\tilde{x}), \quad \Psi_{k,p}(\tilde{x}) = \sum_{i=1}^{d+1} x_{i,k}^{\text{hf,v}} \ell_i^{\text{fe,p}}(\tilde{x}), \quad k = 1, \dots, N_e. \quad (13a)$$

Note that Ψ_k is a polynomial of degree at most κ , while $\Psi_{k,p}$ is a linear map; the latter implies that the image $\mathbb{D}_{k,p} := \Psi_{k,p}(\widehat{\mathbb{D}})$ is a polytope for all $k = 1, \dots, N_e$, and thus

$$\overline{\Omega}_p = \bigcup_{i=1}^{N_e} \overline{\mathbb{D}_{k,p}} \quad (13b)$$

is a polytope and

$$\Psi : \Omega_p \rightarrow \Omega \quad \text{s.t.} \quad \Psi(x)|_{\mathbb{D}_{k,p}} = \Psi_k \left(\Psi_{k,p}^{-1}(x) \right) \quad (13c)$$

is a Lipschitz map from Ω_p to Ω .

The polytope Ω_p and the map Ψ are explicitly derived from the high-order mesh \mathcal{T} : the problem of determining Ω_p and the map Ψ is hence directly linked to the problem of generating a (coarse) high-order mesh \mathcal{T} of the domain of interest. In our framework, the use of high-order discretizations is motivated by two independent considerations. First, coarse-grained meshes with relatively few elements enable rapid searches over the elements and hence guarantee rapid evaluations of the mapping Ψ for new points in Ω_p — this feature is crucial in optimization-based registration as iterative algorithms for (1) require multiple evaluations of (3) for many values of \mathbf{a} . Second, since by construction $\mathbb{N}(x^v; \mathbf{a}) = x^v$ for all vertices x^v of Ω_p and any $\mathbf{a} \in \mathbb{R}^M$ (cf. section 3.2), the reduction of the number of vertices on curved facets of $\partial\Omega$ improves the expressiveness of the ansatz (3).

We observe that the construction of Ψ outlined above might fail for excessively coarse meshes, as shown in the example of Figure 4. Given the domain Ω depicted in Figure 4(a), we might be tempted to consider the coarse mesh in Figure 4(b): even if the curved mesh \mathcal{T} associated with this partition is a proper mesh of Ω , we

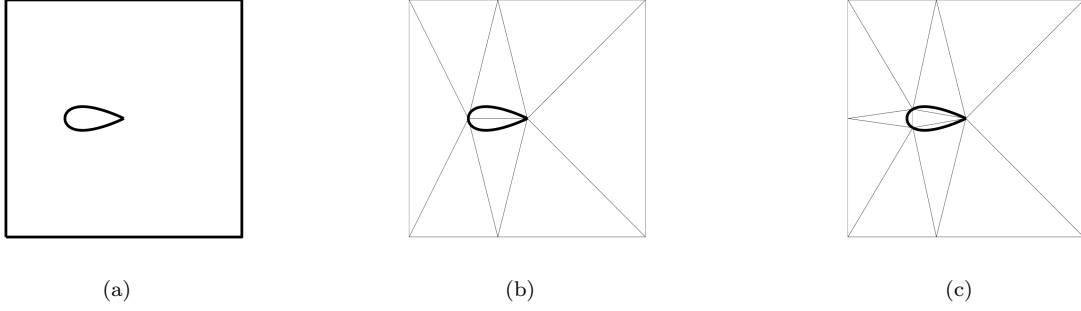


Figure 4: isolated profile in rectangular domain. (a) domain Ω . (b) inadmissible coarse-grained partition.

find that the resulting polytope Ω_p is not isomorphic to Ω up to the boundary (since $\overline{\Omega_p}$ is a rectangle) and Ψ is not continuous up to the boundary of Ω_p . To fix this issue for this geometry, we should consider meshes with at least three points on the profile (cf. Figure 4(c)).

We propose to first prescribe the polytope Ω_p , then determine a linear triangulation \mathcal{T}_p of Ω_p and finally compute the map Ψ by solving a suitable optimization problem. We introduce the parameterizations $\{\gamma_k : (0, 1) \rightarrow \mathbf{F}_k\}_{k=1}^{N_b}$ of the curved edges $\{\mathbf{F}_k\}_{k=1}^{N_b}$ and the Gauss-Lobatto points $\{t_i^{\text{gl}}\}_{i=1}^{\kappa+1} \subset [0, 1]$. Then, we introduce the reference and deformed points

$$x_{j_i, k} = \gamma_k(0)(1 - t_i^{\text{gl}}) + \gamma_k(1) t_i^{\text{gl}}, \quad y_{j_i, k} = \gamma_k(t_i^{\text{gl}}), \quad \text{where } j_{i, k} = i + (k - 1)N_b,$$

for $i = 1, \dots, \kappa + 1$, and $k = 1, \dots, N_b$, and the affine space $\widetilde{\mathcal{W}}_p = \text{id} + \widetilde{\mathcal{U}}_p$ with

$$\widetilde{\mathcal{U}}_p = \left\{ \varphi \in [\mathcal{X}_{\text{hf}, p}]^2 : \varphi \cdot \mathbf{n} \Big|_{\partial\Omega_p \cap \partial\Omega} = 0 \right\}; \quad (14)$$

note that the affine space $\widetilde{\mathcal{W}}_p$ enables deformation of curved facets. In conclusion, we consider the constrained optimization statement:

$$\min_{\Phi \in \widetilde{\mathcal{W}}_p} f_{\text{jac}}(\Phi) + \mathfrak{P}_{\text{brkn}}(\Phi) \quad \text{s.t.} \quad \|\Phi(x_j) - y_j\|_{\infty} \leq \delta, \quad j = 1, \dots, N = (\kappa + 1)N_b, \quad (15)$$

where f_{jac} is designed to enforce the bijectivity of the mapping and is introduced in the next section (cf. (17b)), while $\mathfrak{P}_{\text{brkn}}$ is the quadratic penalty term (12). The penalty (12) was found superior to (11) — that is, it led to more regular meshes and to more rapid convergence of the optimizer — for the model problem of section 5.

The optimization statement (15) reads as a nonlinear non-convex optimization problem with linear inequality constraints; in our numerical implementation, we resort to the Matlab function `fmincon` to solve (15) based on an interior-point method. In the numerical experiments, we consider $\delta = 10^{-6}$.

4.3 Optimization statement

The discussion of sections 4.1 and 4.2 leads to the definition of the search space \mathcal{W} in (1),

$$\mathcal{W} = \left\{ \Phi = \Psi \circ \Phi_p \circ \Psi^{-1} : \Phi_p = \text{id} + \mathcal{U}_p \right\}, \quad (16)$$

where \mathcal{U}_p is defined in (8) and Ψ is defined in (13); here, we discuss the choice of the objective function $f^{\text{obj}} : \mathcal{W} \times \mathcal{P} \rightarrow \mathbb{R}_+$, which should be designed to track coherent structures of the problem and to ensure the bijectivity of the map and/or the properness of the deformed mesh used for the full-order calculations \mathcal{T}_{pb} . We remark that the mesh \mathcal{T}_{pb} is independent of the FE mesh \mathcal{T}_p used in sections 4.1 and 4.2 to define the mapping space, and might also be associated to a different (spectral element, finite volume) discretization method. We denote by $\{\mathcal{D}_k^{\text{pb}}\}_{k=1}^{N_e^{\text{pb}}}$ and $\{\Psi_k^{\text{pb}}\}_{k=1}^{N_e^{\text{pb}}}$ the elements and the elemental mappings of \mathcal{T}_{pb} ; we use notation $\{\Psi_{\Phi, k}^{\text{pb}}\}_{k=1}^{N_e^{\text{pb}}}$ to refer to the elemental mappings of the deformed mesh (see, e.g., [29, Eq. (9)]).

In full generality, we consider the objective function

$$f_{\mu}^{\text{obj}}(\Phi = \Psi \circ \Phi_p \circ \Psi^{-1}) = f_{\mu}^{\text{tg}}(\Phi) + \xi (f_{\text{jac}}(\Phi_p) + f_{\text{msh}}(\Phi) + \mathfrak{P}(\Phi_p)), \quad (17a)$$

where f_{μ}^{tg} is the target function which is introduced below, $\xi > 0$ is a weighting parameter, the penalty \mathfrak{P} is introduced in (11), the function f_{jac} is designed to ensure that the selected map is non-singular,

$$f_{\text{jac}}(\Phi_p) = \frac{1}{|\Omega_p|} \int_{\Omega_p} \exp\left(\frac{\epsilon - J(\Phi_p)}{C_{\text{exp}}}\right) dx, \quad \text{with } \epsilon \in (0, 1), \quad C_{\text{exp}} \ll \epsilon; \quad (17b)$$

the function f_{msh} controls the quality of the deformed mesh

$$f_{\text{msh}}(\Phi) = \frac{1}{|\Omega|} \sum_{k=1}^{N_e^{\text{pb}}} |D_k^{\text{pb}}| \int_{\bar{D}} \exp\left(\frac{q_k^{\text{msh}}(\Phi)}{q_k^{\text{msh}}(\text{id})} - \kappa_{\text{msh}}\right) dx, \quad (17c)$$

where

$$q_k^{\text{msh}}(\Phi) := \frac{1}{d^2} \left(\frac{\|\nabla \Psi_{\Phi,k}^{\text{pb}}\|_{\text{F}}^2}{(\det(\nabla \Psi_{\Phi,k}^{\text{pb}}))_+^{2/d}} \right)^2, \quad d = 2. \quad (17d)$$

We observe that the ratio q_k^{msh} measures the degree of anisotropy of the mesh and it can thus be interpreted as a measure of the quality of the deformed mesh — we recall that the indicator q_k^{msh} was used in [36] in the framework of DG methods. As discussed in [28], the decision to activate the penalty terms f_{jac} and/or f_{msh} depends on the particular way we treat parameterized geometries — map-then-discretize or discretize-then-map: in the numerical experiments, we activate only f_{msh} with $\kappa_{\text{msh}} = 10$.

The target f_{μ}^{tg} measures the degree of similarity between the available estimate of the solution field u_{μ} to the problem of interest and a suitable template solution or template reduced space; f_{μ}^{tg} relies on the introduction of a sensor $s_{\mu} := s_{\mu}(u_{\mu})$ which should highlight the coherent structures we wish to track. We might distinguish between *point-set sensors* and *distributed sensors*. In this work, we combine point-set and distributed sensors to take into account different sources of information and to robustify the greedy procedure outlined in section 4.4. The choice of the sensor might exploit the connection between distributed sensors and the shock sensors that are used to activate artificial viscosities in high-order discretization [19, 20].

Target function based on point-set sensors. Point-set sensors are based on the introduction of a scalar testing function that selects the points of the mesh $\{x_{\mu,j}^*\}_{j=1}^{N_{\mu}^*}$ where the solution u_{μ} satisfies a suitable user-defined criterion (cf. [9]), for any $\mu \in \mathcal{P}$. Given the template point cloud $\{\bar{x}_j^*\}_{j=1}^{\bar{N}^*}$ — which can be prescribed *a priori* or be chosen based on one specific value of the parameters — and the parameter value $\mu \in \mathcal{P}$, we first rely on a standard point-set registration (PSR) procedure (e.g., [18]) that takes as inputs $\{\bar{x}_j^*\}_{j=1}^{\bar{N}^*}$ and $\{x_{\mu,j}^*\}_{j=1}^{N_{\mu}^*}$, to determine the deformed points $\{\hat{x}_{j,\mu}^* = \bar{x}_j^* + v_{j,\mu}^*\}_{j=1}^{\bar{N}^*}$; then, we solve the optimization problem (1) with

$$f_{\mu}^{\text{tg}}(\Phi) = \frac{1}{\bar{N}^*} \sum_{i=1}^{\bar{N}^*} \|\Phi(\bar{x}_i^*) - \hat{x}_{i,\mu}^*\|_2^2. \quad (18)$$

As discussed in [9] and also [28], we can interpret the solution to (1) with objective (17)-(18) as an approximate projection of the mapping returned by the PSR procedure — which is neither guaranteed to map the boundary of the domain Ω in itself nor to be globally bijective — onto the space of admissible bijections in Ω .

In order to speed up calculations, it is important to exploit the structure of the mapping in (3) and precompute Ψ^{-1} where needed before calling the optimizer. In more detail, in order to speed up the evaluation of f_{μ}^{tg} in (18), we first compute and store $\bar{z}_j^* = \Psi^{-1}(\bar{x}_j^*)$ for $j = 1, \dots, \bar{N}^*$ and then we evaluate (18) as

$$f_{\mu}^{\text{tg}}(\Phi) = \frac{1}{\bar{N}^*} \sum_{i=1}^{\bar{N}^*} \|\Psi(\Phi_{\text{p}}(\bar{z}_i^*)) - \hat{x}_{i,\mu}^*\|_2^2.$$

Similar reasoning can be exploited for the evaluation of (17c).

Target function based on distributed sensors. A distributed sensor is a function of the solution field u_{μ} that highlights the features of u_{μ} that we wish to track. Given the reduced n -dimensional space \mathcal{Z}_n embedded in a Hilbert space \mathcal{X} defined over Ω , we observe that in model reduction the parametric mapping Φ should minimize the target

$$f_{\mu}^{\text{tg,opt}}(\Phi) := \min_{\zeta \in \mathcal{Z}_n} \int_{\Omega} \|u_{\mu} \circ \Phi - \zeta\|_2^2 dx, \quad (19)$$

over all values of μ in \mathcal{P} : $f_{\mu}^{\text{tg,opt}}(\Phi)$ is the projection error in the mapped configuration. Note that $f_{\mu}^{\text{tg,opt}}$ depends on the choice of the reduced space \mathcal{Z}_n whose selection is inherently coupled with the problem of finding Φ : we postpone the procedure for the construction of the reduced space to the next section.

The explicit use of the solution u_{μ} in the optimization statement (1) is computationally unfeasible and prone to instabilities: first, the solution u_{μ} is typically defined over an unstructured grid for which function evaluation at the deformed quadrature points $\{\Phi(x_q^{\text{qd}})\}_{q=1}^{N_q^{\text{qd}}}$ is extremely expensive; second, we might exploit prior knowledge about the problem of interest to identify a scalar function of u_{μ} that better isolates the features

we wish to track (e.g., shocks) using registration, from the features we expect to be able to approximate through a linear expansion of (mapped) snapshots.

Exploiting the form of Φ , and the change-of-variable $x = \Psi(\xi)$, we find

$$\int_{\Omega} \|u_{\mu} \circ \Phi - \zeta\|_2^2 dx = \int_{\Omega_p} \|u_{\mu} \circ \Psi \circ \Phi_p - \zeta \circ \Psi^{-1}\|_2^2 J(\Psi) d\xi.$$

If we replace $u_{\mu} \circ \Psi$ with a scalar sensor s_{μ} defined over the domain Ω_p and the reduced space \mathcal{Z}_n for the solution with a space (dubbed *template space*) $\mathcal{S}_n \subset L^2(\Omega_p)$ for the sensor, we obtain

$$f_{\mu}^{\text{tg}}(\Phi) := \min_{\nu \in \mathcal{S}_n} \int_{\Omega_p} |s_{\mu} \circ \Phi_p - \nu|^2 J(\Psi) dx, \quad (20)$$

which is the target function employed in the numerical experiments.

From the definition (20), we deduce that computation of $f_{\mu}^{\text{tg}}(\Phi)$ requires to evaluate s_{μ} in the deformed quadrature points $\{\Phi_p(x_q^{\text{d},p})\}_q$ of the mesh \mathcal{T}_p at each iteration of the optimization algorithm for (1). To speed up the evaluation of the objective function, we propose to define the sensor s_{μ} over a tensorized structured grid \mathcal{T}_{box} of the minimal rectangle Ω_{box} that contains Ω_p , with axes parallel to the axes of the coordinate system. In order to define s_{μ} , we proceed as follows: first, we define a scalar function g of u_{μ} (e.g., Mach number, Reynolds number, vorticity, kinetic energy) and we evaluate $g(u_{\mu})$ in all points $x_1^{\text{box}}, \dots, x_{N_{\text{box}}}^{\text{box}}$ of the mesh \mathcal{T}_{box} that are contained in Ω_p ; second, if we denote by $\mathcal{S}_{\text{hf}} \subset L^2(\Omega_{\text{box}})$ the FE space associated with the mesh \mathcal{T}_{box} , we solve the constrained optimization problem

$$\min_{s \in \mathcal{S}_{\text{hf}}} \int_{\Omega_{\text{box}}} \|\nabla s\|_2^2 dx \quad \text{s.t.} \quad s(x_i^{\text{box}}) = g(u_{\mu}(\Psi(x_i^{\text{box}}))), \quad i = 1, \dots, N_{\text{box}}. \quad (21)$$

Since $g(u_{\mu})$ might exhibit sharp gradients due to the presence of boundary/internal layers and/or shocks or contact discontinuities, we here rely on low-order ($p = 1$) FE approximations and we also consider the application of a low-pass filter to avoid spurious oscillations that might be generated during the interpolation between the two meshes.

4.4 Construction of the parametric map

The target function (20) depends on the template space $\mathcal{S}_n \subset L^2(\Omega_p)$. Following [29, 30], given a set of sensor snapshots $\{s_{\mu} : \mu \in \mathcal{P}_{\text{train}}\}$ with $\mathcal{P}_{\text{train}} = \{\mu^k\}_{k=1}^{n_{\text{train}}}$, we propose to rely on an iterative procedure that performs registration over the entire training set and then exploits the results to update the template space \mathcal{S}_n in a greedy fashion. Below, we denote by $\Phi_{\mu}^* = \Psi \circ \Phi_{p,\mu}^* \circ \Psi^{-1}$ the solution to the optimization problem (1) for the parameter $\mu \in \mathcal{P}$, with $\Phi_{p,\mu}^* = \text{id} + \varphi_{p,\mu}^*$. Furthermore, given the m -dimensional subspace $\mathcal{U}_m \subset \mathcal{U}_p$, we define the reduced-order basis (ROB) $\mathbf{w}_m : \mathbb{R}^m \rightarrow \mathcal{U}_p$ such that $\|\mathbf{w}_m \mathbf{a}\| = \|\mathbf{a}\|_2$ where $\|\cdot\| = \sqrt{(\cdot, \cdot)}$ is defined in (10); we also denote by $\mathbf{a}_{\mu}^* \in \mathbb{R}^m$ the optimal mapping coefficients associated with Φ_{μ}^* , that is $\varphi_{p,\mu}^* = \mathbf{w}_m \mathbf{a}_{\mu}^*$.

Algorithm 1 summarizes the computational procedure. We use notation

$$[\mathbf{a}_{\mu}^*, f_{\mu}^*] = \text{registration}(s_{\mu}, \mathcal{S}_n, \mathbf{w}_m, \mathcal{T}_{\text{pb}}, \Psi, \mathbf{a}_{\mu}^0)$$

to refer to the function that takes as inputs (i) the target sensor $s_{\mu} : \Omega_p \rightarrow \mathbb{R}$, (ii) the template space \mathcal{S}_n , (iii) the ROB \mathbf{w}_m associated with the mapping space $\mathcal{U}_m \subset \mathcal{U}_p$, (iv) the mesh \mathcal{T}_{pb} , (v) the geometric mapping $\Psi : \Omega_p \rightarrow \Omega$ and (vi) the initial guess $\mathbf{a}_{\mu}^0 \in \mathbb{R}^m$ for the optimizer, and returns (I) the mapping coefficients \mathbf{a}_{μ}^* associated with a local minimum Φ_{μ}^* of the problem

$$\min_{\Phi \in \mathcal{W}_m} f_{\mu}^{\text{obj}}(\Phi) \quad \text{where} \quad \mathcal{W}_m = \{\Phi = \Psi \circ \Phi_p \circ \Psi^{-1} : \Phi_p \in \text{id} + \mathcal{U}_m\} \subset \mathcal{W},$$

where \mathcal{W} is defined in (16), and (II) the value of the target function $f_{\mu}^* = f_{\mu}^{\text{tg}}(\Phi_{\mu}^*)$. Note that $f_{\mu}^{\text{obj}} : \mathcal{W} \rightarrow \mathbb{R}_+$ depends on the mesh \mathcal{T}_{pb} through the term f_{mesh} in (17c). We also introduce the function

$$[\mathbf{w}_m, \{\mathbf{a}_{\mu}^{\text{proj}}\}_{\mu \in \mathcal{P}_{\text{train}}}] = \text{POD}(\{\mathbf{a}_{\mu}^*\}_{\mu \in \mathcal{P}_{\text{train}}}, \text{tol}_{\text{pod}}, (\cdot, \cdot)_2),$$

which implements proper orthogonal decomposition (POD, [25, 32]) based on the method of snapshots with Euclidean inner product $(\cdot, \cdot)_2$: the tolerance $\text{tol}_{\text{pod}} > 0$ drives the selection of the number of modes m based on the energy criterion

$$m := \min \left\{ m' : \sum_{j=1}^{m'} \lambda_j \geq (1 - \text{tol}_{\text{pod}}) \sum_{i=1}^{n_{\text{train}}} \lambda_i \right\}, \quad (22)$$

where $\lambda_1 \geq \dots \geq \lambda_{n_{\text{train}}} \geq 0$ are the eigenvalues of the Gramian matrix $\mathbf{C} \in \mathbb{R}^{n_{\text{train}} \times n_{\text{train}}}$ such that $(\mathbf{C})_{k,k'} = (\varphi_{\mathbf{p},\mu^k}^*, \varphi_{\mathbf{p},\mu^{k'}}^*) = \mathbf{a}_{\mu^k}^* \cdot \mathbf{a}_{\mu^{k'}}^*$. The function POD returns also the mapping coefficients associated with the projected displacements $W_m \mathbf{a}_\mu^{\text{proj}} = \Pi_{\mathcal{U}_m} \varphi_{\mathbf{p},\mu}^*$; the latter are used to initialize the iterative method for the optimization problem for the subsequent iterations.

Algorithm 1 Registration algorithm

Inputs: $\{s_\mu : \mu \in \mathcal{P}_{\text{train}}\}$ snapshot set, $\mathcal{S}_{n_0} = \text{span}\{s_{\mu^{*,(i)}}\}_{i=1}^{n_0}$ initial template space; \mathcal{T}_{pb} mesh for HF computations.

Outputs: \mathcal{S}_n template space, $W_m : \mathbb{R}^m \rightarrow \mathcal{U}_m$ mapping ROB, $\{\varphi_{\mathbf{p},\mu^k}^* = W_m \mathbf{a}_{\mu^k}^*\}_k$ optimal mappings.

- 1: Initialization: $\mathcal{S}_{n=n_0} = \mathcal{S}_{n_0}$, $\Xi_\star = \{\mu^{*,(i)}\}_{i=1}^{n_0}$, $\mathcal{U}_m = \mathcal{U}_{\mathbf{p}}$ (cf. (8)).
 - 2: **for** $n = n_0, \dots, n_{\text{max}} - 1$ **do**
 - 3: $[\mathbf{a}_\mu^*, \mathbf{f}_\mu^*] = \text{registration}(s_\mu, \mathcal{S}_n, W_m, \mathcal{T}_{\text{pb}}, \Psi, \mathbf{a}_\mu^0)$ for all $\mu \in \mathcal{P}_{\text{train}}$ *see Remark 4.1 for definition of \mathbf{a}_μ^0*
 - 4: $[W_m, \{\mathbf{a}_\mu^{\text{proj}}\}_{\mu \in \mathcal{P}_{\text{train}}}] = \text{POD}(\{\mathbf{a}_\mu^*\}_{\mu \in \mathcal{P}_{\text{train}}}, \text{tol}_{\text{pod}}, (\cdot, \cdot)_2)$,
 - 5: **if** $\max_{\mu \in \mathcal{P}_{\text{train}}} \mathbf{f}_\mu^* < \text{tol}$ **then**
 - 6: **break**
 - 7: **else**
 - 8: $\Xi_\star = \Xi_\star \cup \{\mu^{*,(n+1)}\}$ with $\mu^{*,(n+1)} = \arg \max_{\mu \in \mathcal{P}_{\text{train}}} \mathbf{f}_\mu^*$.
 - 9: $\mathcal{S}_{n+1} = \text{span}\{s_{\mu^{*,i}} \circ \Phi_{\mathbf{p},\mu^{*,i}}^*\}_{i=1}^{n+1}$.
 - 10: **end if**
 - 11: **end for**
-

Remark 4.1. Further implementation details. Since the optimization problem is highly non-convex, the choice of the initial condition is extremely important to avoid convergence to unsatisfactory local minima. For $n = n_0 + 1, n_0 + 2, \dots, n_{\text{max}} - 1$, we simply use $\mathbf{a}_\mu^0 = \mathbf{a}_\mu^{\text{proj}}$ (cf. Line 4). On the other hand, for the first iteration, we first reorder the parameters in $\mathcal{P}_{\text{train}}$ so that $\mu^{(1)} = \arg \min_{\mu \in \mathcal{P}_{\text{train}}} \|\mu - \mu^{*,(1)}\|_2$ and

$$\mu^{(k)} = \arg \min_{\mu \in \mathcal{P}_{\text{train}} \setminus \{\mu^{(i)}\}_{i=1}^{k-1}} \left(\min_{\mu' \in \{\mu^{(i)}\}_{i=1}^{k-1}} \|\mu - \mu'\|_2 \right), \quad k = 2, \dots, n_{\text{train}};$$

then, we choose the initial condition as follows:

$$\mathbf{a}_{\mu^{(1)}}^0 = 0, \quad \mathbf{a}_{\mu^{(k)}}^0 = \widehat{\mathbf{a}}_{\mu^{(\text{ne}_k)}} \quad \text{with } \text{ne}_k = \arg \min_{j=1, \dots, k-1} \|\mu^{(j)} - \mu^{(k)}\|_2,$$

for $k = 2, \dots, n_{\text{train}}$. In a previous implementation of the procedure, we also included box constraints in the optimization statement (cf. [27, section 3.1.2]) to control the sensitivity of the mapping coefficients to parameter variations;

$$\|\mathbf{a}_{\mu^{(k)}}^* - \mathbf{a}_{\mu^{(k)}}^0\|_\infty \leq C_\infty \|\mu^{(k)} - \mu^{(\text{ne}_k)}\|_2, \quad \text{with } C_\infty = 10; \quad (23)$$

however, in the numerical experiments of the present work, we found that the solution to the unconstrained problem satisfied the constraints (23) for all the experiments considered. We further observe that Algorithm 1 depends on several hyper-parameters. In our tests, we set $\mathcal{S}_{n_0=1} = \text{span}\{s_{\bar{\mu}}\}$, where $\bar{\mu}$ is the centroid of \mathcal{P} ; furthermore, we set $n_{\text{max}} = 6$, $\text{tol}_{\text{pod}} = 5 \cdot 10^{-3}$ and $\text{tol} = 10^{-4}$.

Remark 4.2. Generalization. Given the dataset $\{(\mu^k, \mathbf{a}_{\mu^k}^*)\}_{k=1}^{n_{\text{train}}}$ as provided by Algorithm 1, we resort to a multi-target regression algorithm to learn a regressor $\mu \mapsto \widehat{\mathbf{a}}_\mu$ for the mapping coefficients, and ultimately define the parametric mapping

$$\Phi : \Omega \times \mathcal{P} \rightarrow \Omega, \quad \Phi_\mu := \Psi \circ \Phi_{\mathbf{p},\mu} \circ \Psi^{-1}, \quad \text{with } \Phi_{\mathbf{p},\mu} = \mathbf{i}d + W_m \widehat{\mathbf{a}}_\mu, \quad (24)$$

We here resort to radial basis function (RBF, [33]) approximation: other regression algorithms could also be considered. Similarly to [27, 30], to avoid overfitting, we verify the statistical significance of the RBF estimators. We randomly split the dataset $\{(\mu^k, \mathbf{a}_{\mu^k}^*)\}_{k=1}^{n_{\text{train}}}$ into the learning and test sets $\{(\mu^k, \mathbf{a}_{\mu^k}^*)\}_{k=1}^{n_{\text{learn}}}$ and $\{(\mu^j, \mathbf{a}_{\mu^j}^*)\}_{j=1}^{n_{\text{test}}}$ (we here consider a 80%-20% learning/test split); we compute the RBF approximation $\widehat{\mathbf{a}} : \mathcal{P} \rightarrow \mathbb{R}^m$ based on the learning set and we compute the out-of-sample R-squared coefficient for each component:

$$R_i^2 = 1 - \frac{\sum_{j=1}^{n_{\text{test}}} (\mathbf{a}_{\mu^j}^* - \widehat{\mathbf{a}}_{\mu^j})_i^2}{\sum_{j=1}^{n_{\text{test}}} (\mathbf{a}_{\mu^j}^* - \bar{\mathbf{a}})_i^2}, \quad \bar{\mathbf{a}} = \frac{1}{n_{\text{learn}}} \sum_{k=1}^{n_{\text{learn}}} \mathbf{a}_{\mu^k}^*, \quad i = 1, \dots, m. \quad (25)$$

Then, we retain exclusively modes for which R_i^2 is above the threshold $R_{\text{min}} = 0.70$.

Remark 4.3. Parametric registration based on point-set sensors. *The greedy procedure in Algorithm 1 is motivated by the need to construct the template space \mathcal{S}_n . If we rely on point-set sensors, we do not have to perform multiple iterations. However, we empirically found that performing two iterations of the for loop in Algorithm 1 does not hinder computational efficiency — since the cost is dominated by the high-dimensional registration problems solved during the first iteration — and has a beneficial effect on generalization outside the training set.*

5 Application to an inviscid flow past an array of LS89 turbine blades

We consider the problem of estimating the solution to the two-dimensional Euler equations past an array of LS89 turbine blades.

5.1 Model problem

We consider the computational domain depicted in Figure 7(a); we prescribe total temperature, total pressure and flow direction at the inflow, static pressure at the outflow, non-penetration condition on the blade and periodic boundary conditions on the lower and upper boundaries. We study the sensitivity of the solution with respect to two parameters: the free-stream Mach number Ma_∞ and the height of the channel H , $\mu = [\text{Ma}_\infty, H]$. We consider the parameter domain $\mathcal{P} = [0.95, 1.05] \times [0.9, 0.95]$. We refer to [2] for a detailed presentation of the employed nondimensionalization, HF DG formulation and pseudo-transient continuation strategy.

Figure 5 shows the distribution of the Mach field for $\mu_{\min} = [0.95, 0.9]$ and $\mu_{\max} = [1.05, 0.95]$; Figure 6(a) shows the behavior of the Mach number on the upper side of the blade for four parameter values, while Figure 6(b) shows the behavior of the entropy profile $E = \log(p) - \gamma \log(\rho)$ where p is the pressure field, $\gamma = 1.4$ is the ratio of specific heats, and ρ is the density field. The solution develops a normal shock on the upper side of the blade for sufficiently large values of Ma_∞ and H ; furthermore, the entropy E exhibits several peaks that correspond to the blade wakes. The solution develops two shocks at the trailing edge, which are highly undesirable for turbomachinery applications: we expect that at the trailing edge viscous effects might not be negligible; for this reason, a more thorough investigation should rely on a model that accounts for viscous effects. We observe that the shock location and the entropy peaks are sensitive to the value of the parameter: this justifies the application of registration procedures.

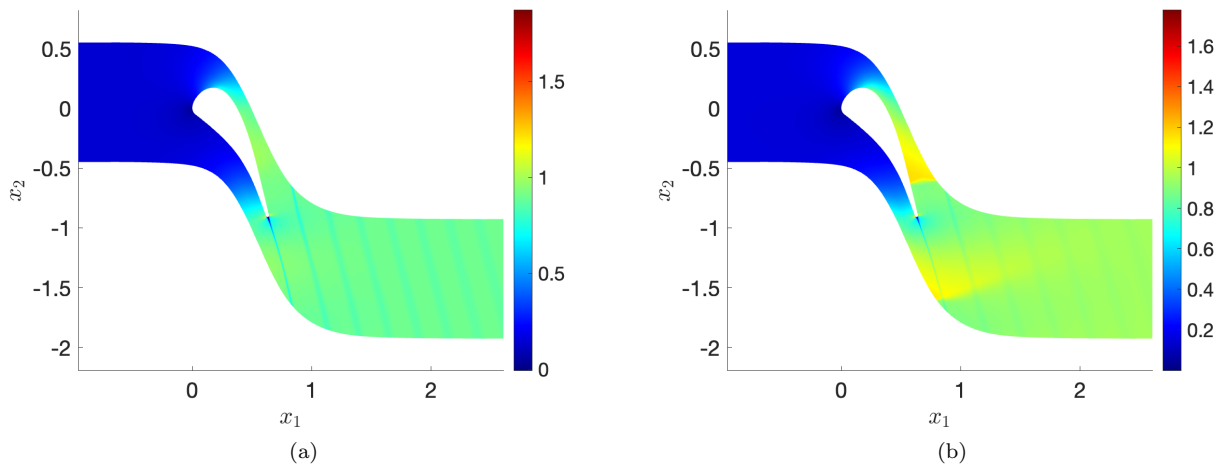


Figure 5: inviscid flow past an array of LS89 turbine blades. (a)-(b) Mach field for $\mu = [0.95, 0.9]$ and $\mu = [1.05, 0.95]$.

5.2 Definition of the mapping ansatz

We deal with geometry variations through a piecewise-smooth mapping associated with the partition in Figure 7(b). We set $H_{\text{ref}} = 1$ and we define the curve $x_1 \mapsto f_{\text{btm}}(x_1)$ that describes the lower boundary Γ_{btm} of the domain $\Omega = \Omega(H = 1)$; then, we define $\tilde{H} > 0$ such that $x_1 \mapsto f_{\text{btm}}(x_1) + \tilde{H}$ and $x_1 \mapsto f_{\text{btm}}(x_1) + H - \tilde{H}$ do

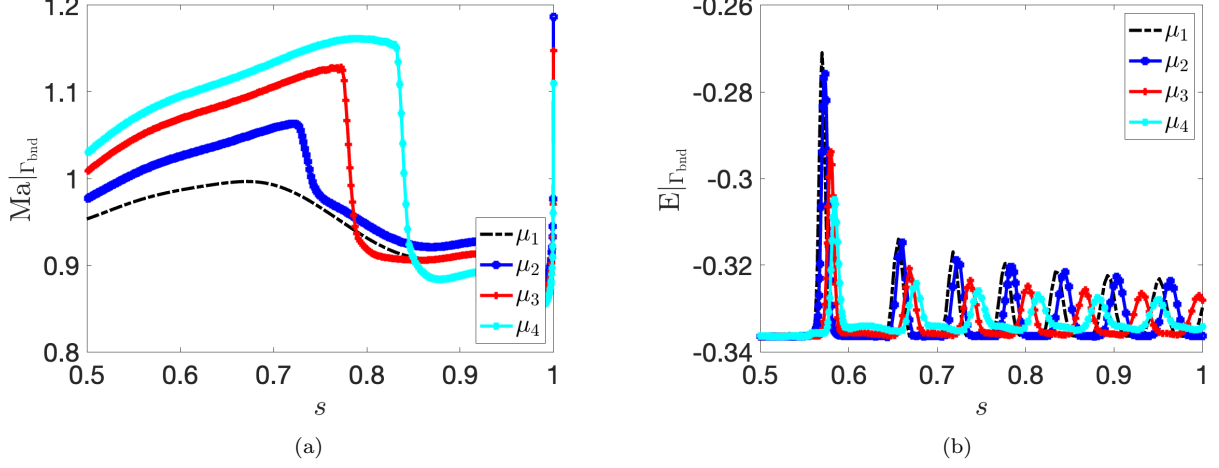


Figure 6: inviscid flow past an array of LS89 turbine blades. (a) Mach profile over the upper side of the blade for four values of the parameter in \mathcal{P} . (b) entropy profile on the bottom boundary for four values of the parameter in \mathcal{P} . The parameter s denotes the normalized curvilinear coordinate, $s \in [0, 1]$.

not intersect the blade for any $H \in [0.95, 1.05]$; finally, we define the geometric mapping

$$\Psi_H^{\text{geo}}(x = [x_1, x_2]) = \begin{bmatrix} x_1 \\ \psi_H^{\text{geo}}(x) \end{bmatrix}, \quad (26a)$$

where

$$\psi_H^{\text{geo}}(x) = \begin{cases} o_1(x_1) + C(H)(x_2 - o_1(x_1)) & x_2 < o_1(x_1), \\ o_2(x_1) + C(H)(x_2 - o_2(x_1)) & x_2 > o_2(x_1), \\ x_2 & \text{otherwise,} \end{cases} \quad (26b)$$

with $o_1(x_1) = f_{\text{btm}}(x_1) + \tilde{H}$, $o_2(x_1) = f_{\text{btm}}(x_1) + H_{\text{ref}} - \tilde{H}$ and $C(H) = \frac{H - H_{\text{ref}}}{2\tilde{H}} + 1$. Then, we consider computational maps (3) from the domain $\Omega = \Omega(H = H_{\text{ref}})$ to $\Omega_\mu = \Omega(H)$ such that

$$\mathbf{N}(x, \mathbf{a}, \mu) = \Psi_H^{\text{geo}} \circ \Psi \circ \mathbf{N}_p(\mathbf{a}) \circ \Psi^{-1}(x), \quad (27)$$

for a proper choice of the mapping Ψ and the polytope Ω_p . Note that $\tilde{\mathbf{N}}(\mathbf{a}) = \Psi \circ \mathbf{N}_p(\mathbf{a}) \circ \Psi^{-1}$ defines a map from Ω in itself.

The polytope Ω_p and the mapping $\Psi : \Omega_p \rightarrow \Omega$ should be designed to ensure the periodicity constraint

$$\mathbf{N}(x + [0, H_{\text{ref}}], \mathbf{a}, \mu) = \mathbf{N}(x, \mathbf{a}, \mu) + [0, H], \quad \forall x \in \Gamma_{\text{btm}}. \quad (28)$$

The geometric mapping Ψ^{geo} satisfies the periodicity constraint; it is thus sufficient to enforce that $\tilde{\mathbf{N}}(x + [0, H_{\text{ref}}], \mathbf{a}, \mu) = \tilde{\mathbf{N}}(x, \mathbf{a}, \mu) + [0, H_{\text{ref}}]$ for all $x \in \Gamma_{\text{btm}}$. Towards this end, (i) we define the polytope Ω_p with vertices V such that $V \cap \Gamma_{\text{btm},p} = V \cap \Gamma_{\text{top},p} + [0, H_{\text{ref}}]$, where $\Gamma_{\text{btm},p}, \Gamma_{\text{top},p}$ denote the lower and upper boundaries of the polytope; (ii) we define the linear mesh \mathcal{T}_p in Figure 7(c) with matching nodes on the periodic boundaries²; (iii) we define the mapping Ψ by solving (15) in the affine space $\tilde{\mathcal{W}}_p = \{\text{id} + \varphi \in [\mathcal{X}_{\text{hf},p}]^2 : \varphi \cdot \mathbf{n}|_{\partial\Omega_p \cap \partial\Omega} = 0, \varphi|_{\Gamma_{\text{btm},p}} = \varphi|_{\Gamma_{\text{top},p}}\}$ and we set \mathcal{U}_p (cf. (8)) as $\mathcal{U}_p = \{\varphi \in [\mathcal{X}_{\text{hf},p}]^2 : \varphi \cdot \mathbf{n}|_{\partial\Omega_p} = 0, \varphi|_{\Gamma_{\text{btm},p}} = \varphi|_{\Gamma_{\text{top},p}}\}$. The resulting curved mesh is provided in Figure 7(d); in the experiments, we consider polynomials of degree ten, which implies $M = 1359$. Note that, since $\tilde{\mathcal{W}}_p$ and \mathcal{U}_p are spaces of piecewise polynomials, it suffices to enforce the periodicity constraint at mesh nodes.

5.3 Definition of the sensor

We consider a target function f_μ^{tg} that combines a point-set sensor and a distributed sensor

$$f_\mu^{\text{tg}} = \frac{1}{4} \sum_{i=1}^4 \|\mathbf{N}(\tilde{x}_i, \mathbf{a}, \mu) - \hat{x}_{i,\mu}\|_2^2 + \min_{\nu \in \mathcal{S}_n} \int_{\Omega_p} |s_\mu \circ \mathbf{N}_p(\mathbf{a}) - \nu|^2 J(\Psi) dx, \quad (29)$$

²The same condition is enforced in the HF mesh.

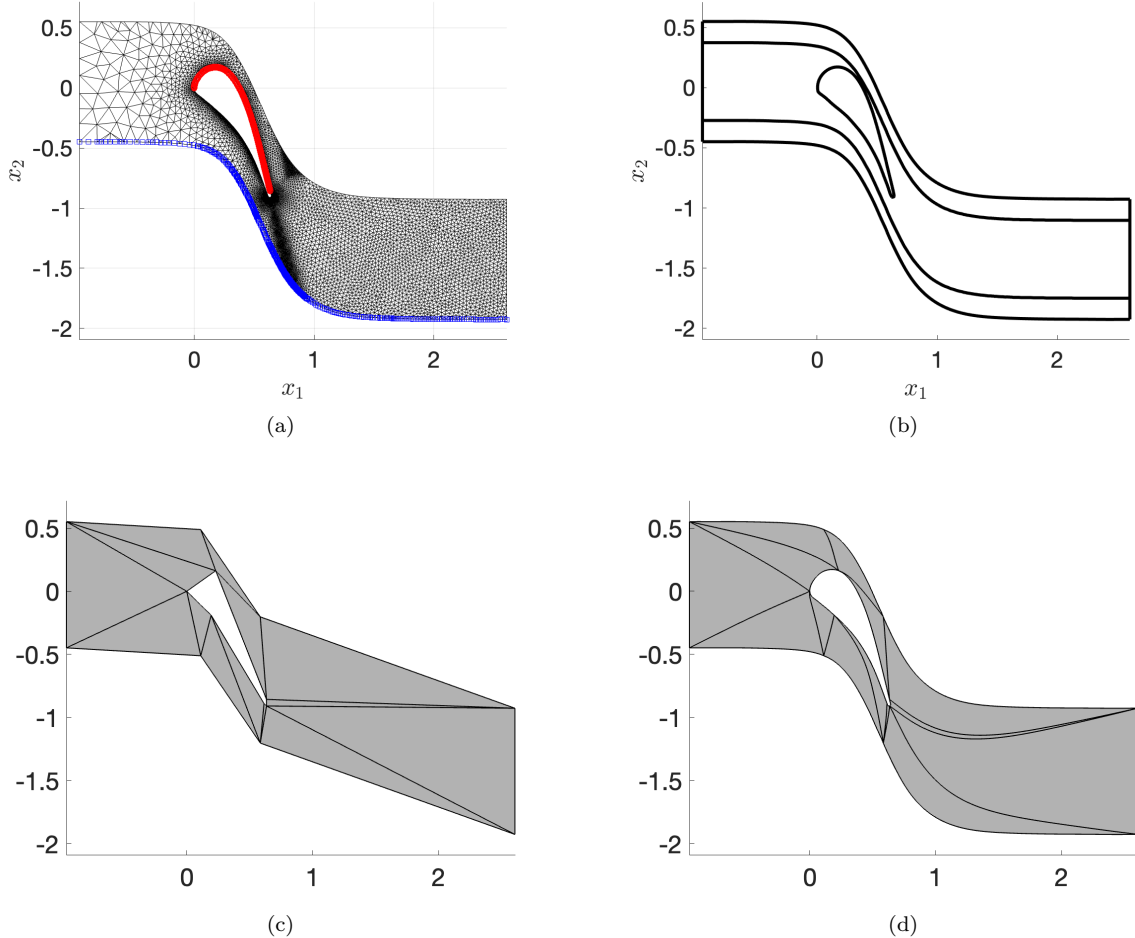


Figure 7: inviscid flow past an array of LS89 turbine blades. (a) computational mesh \mathcal{T}_{pb} for DG calculations; red dots denote the nodes on the upper blade side; blue squares denote the nodes on the lower boundary. (b) partition associated with the geometric map (26). (c)-(d) coarse-grained linear mesh \mathcal{T}_p and curved mesh \mathcal{T} for registration.

where the distributed sensor s_μ is obtained from the Mach field using (21), the template space \mathcal{S}_n is built adaptively using Algorithm 1, and the salient points $\{\hat{x}_{i,\mu}\}_i$ correspond to the first three peaks of the entropy profile on the lower boundary (cf. Figure 6(b)) and the shock location on the upper boundary (cf. Figure 6(a)).

We identify the entropy peaks by computing the local maxima of the entropy profile on $\Gamma_{\text{btm},\mu}$. We detect the shock location on the upper blade side using the following procedure: first, we compute the mean values $\{\overline{\text{Ma}}_j\}_j$ and $\{\overline{d\text{Ma}}_j\}_j$ of the Mach number and its tangential derivative on each facet $\{F_j\}_j$ of the select boundary; second, we find the index j^* such that $\overline{\text{Ma}}_{j^*} > 1 > \overline{\text{Ma}}_{j^*+1}$ and $\overline{d\text{Ma}}_{j^*} < -\frac{10^{-2}}{|F_{j^*}|}$ and we return the estimate $x_{\text{shk},\mu}^{\text{raw}}$ equal to the midpoint of the selected facet.

Given the raw estimates $\{x_{i,\mu}^{\text{raw}} : i = 1, \dots, 4, \mu \in \mathcal{P}_{\text{train}}\}$ of the point sensors, we apply radial basis function (RBF) regression to find smoother estimates that facilitate the generalization step (cf. Remark 4.2); in order to ensure that the points are on the boundary, we apply RBF to the curvilinear coordinates of the points. As shown in Figure 6(a), the solution does not exhibit any shock for several parameter values; we do not consider these points to train the RBF surrogate, and we rely on the surrogate itself to find a fictitious estimate of $\hat{x}_{\text{shk},\mu}$ for all $\mu \in \mathcal{P}$.

5.4 Performance of the registration procedure

We apply Algorithm 1 based on a regular 11×6 grid of parameters $\mathcal{P}_{\text{train}}$. Figure 8 compares the location of the sensors $\{\hat{x}_{i,\mu} = (\Psi_H^{\text{geo}})^{-1}(\hat{x}_{i,\mu}) : i = 1, \dots, 4, \mu \in \mathcal{P}_{\text{train}}\}$ and their mapped counterparts $\{\hat{x}'_{i,\mu} = \Phi_\mu^{-1}(\hat{x}_{i,\mu}) : i = 1, \dots, 4, \mu \in \mathcal{P}_{\text{train}}\}$; similarly, Figure 9 reproduces the results in Figure 6 for the mapped solution field. We observe that the peaks of the mapped entropy field on Γ_{btm} and the shock on the upper side of the blade are nearly insensitive to the parameter value. For all in-sample and out-of-sample configurations considered, the quality of the deformed mesh — which is measured by (17d) — is comparable with the one of the original

mesh.

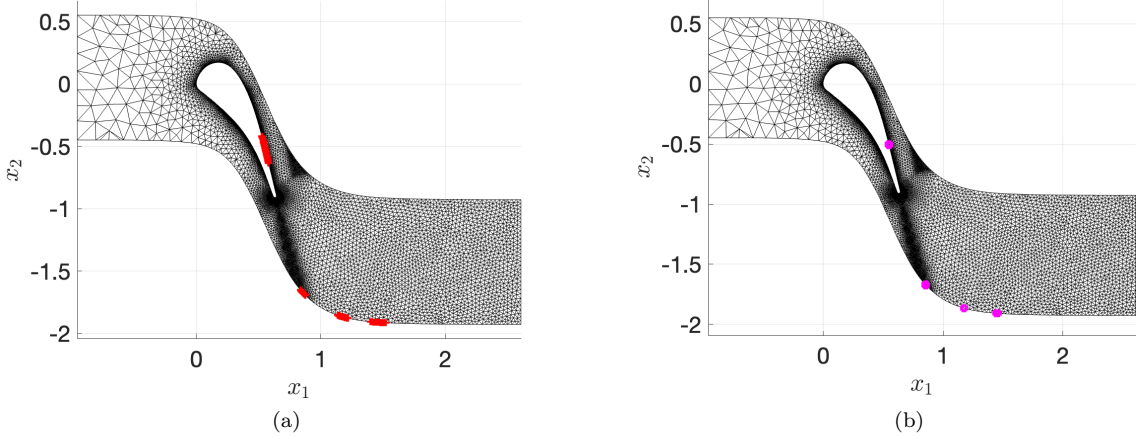


Figure 8: inviscid flow past an array of LS89 turbine blades. (a) sensor points used in the registration procedure for $n_{\text{train}} = 66$ configurations. (b) mapped sensor points.

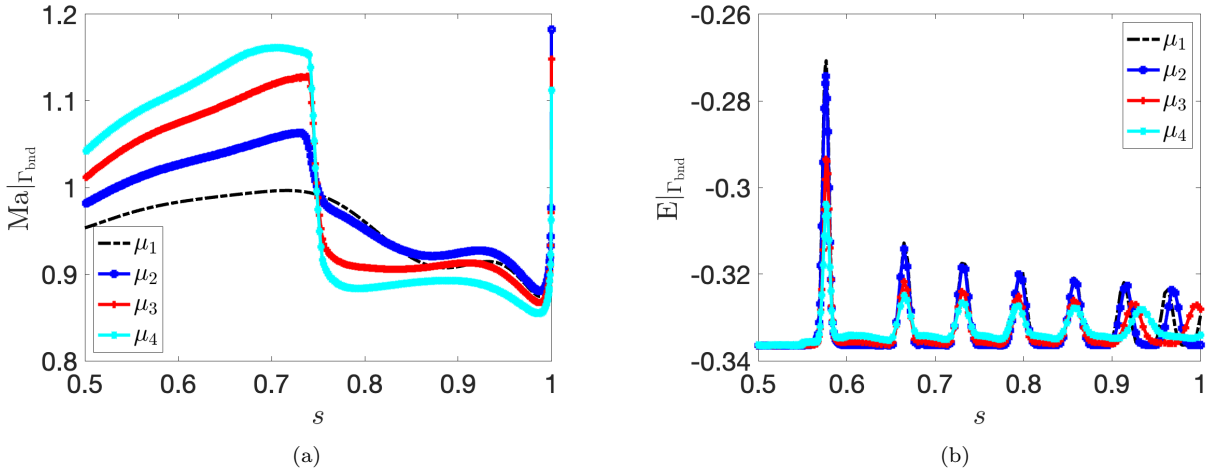


Figure 9: inviscid flow past an array of LS89 turbine blades. (a) mapped Mach profile over the upper side of the blade for four values of the parameter in \mathcal{P} . (b) mapped entropy profile on the bottom boundary for four values of the parameter in \mathcal{P} .

5.5 Model reduction

We rely on POD+regression to estimate the solution field. POD solution coefficients are estimated using the same RBF regression method that is employed for the mapping coefficients (cf. Remark 4.2). To assess performance, we consider a dataset of $n_{\text{test}} = 20$ randomly-selected parameters $\mathcal{P}_{\text{test}}$ and we compute the L^2 maximum relative errors

$$E_{\max} = \max_{\mu \in \mathcal{P}_{\text{test}}} \frac{\|\hat{u}_{\mu} - u_{\mu}^{\text{hf}}\|_{L^2(\Omega_{\mu})}}{\|u_{\mu}^{\text{hf}}\|_{L^2(\Omega_{\mu})}}, \quad E_{\max}^{\text{bnd}} = \max_{\mu \in \mathcal{P}_{\text{test}}} \frac{\|\hat{u}_{\mu} - u_{\mu}^{\text{hf}}\|_{L^2(\Gamma_{\text{bld}})}}{\|u_{\mu}^{\text{hf}}\|_{L^2(\Gamma_{\text{bld}})}}, \quad (30)$$

where Γ_{bld} denotes the boundary of the blade. Figure 10 shows the results for the “linear” ROM and the “registered” ROM — both approaches involve the application of a geometric mapping; the difference is that for the linear ROM the mapping is chosen a priori and corresponds to Ψ^{geo} (26), while for the registered ROM the mapping is chosen through the registration procedure discussed in the paper. Both linear and registered ROMs reach a plateau for $n \approx 10$ due to the limited amount of datapoints. We observe that registration improves performance by a factor 2.04 for the global error and a factor 8.04 for the error on the blade, for the same amount of HF data.

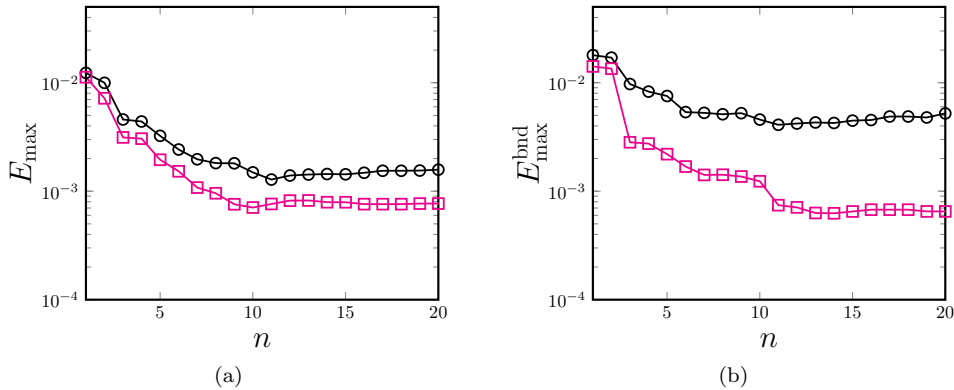


Figure 10: inviscid flow past an array of LS89 turbine blades; model reduction. Behavior of the out-of-sample errors (30) for the linear ROM $\text{---}\circ\text{---}$ and the registered ROM $\text{---}\square\text{---}$ for $n_{\text{train}} = 66$ and several values of n .

6 Summary and discussion

We addressed the problem of parametric registration for manifolds associated to the solution to parametric PDEs: registration is designed to track coherent structures of the solution field, and ultimately simplify the task of parametric MOR. We proposed and analyzed a new class of compositional maps (3) for registration in two-dimensional domains. We provided sufficient conditions to ensure the bijectivity of the mapping Φ (cf. Proposition 2.1 and Corollary 2.3) and we studied the approximation properties: we found that the ansatz (3) is dense in a meaningful subspace of diffeomorphisms only for polytopal domains (Corollary 2.5, Lemma 3.2); on the other hand, the multi-layer generalization (4) is dense for arbitrary domains under the assumption of small deformation (cf. Lemma 3.3). We discussed an actionable procedure to determine the ansatz (3) for arbitrary domains, which exploits a coarse-grained high-order FE mesh; finally, we illustrated the performance of the method for a parametric compressible flow past a cascade of turbine blades.

We aim to extend our approach in several directions. First, we aim to extend Proposition 2.1 to (a class of) Lipschitz maps. Second, we wish to automate the construction of the polytope Ω_p ; we also wish to devise effective implementations of the ansatz (4). Third, we wish to extend our method to three-dimensional domains: this extension likely requires the development of specialized optimization routines to cope with high-dimensional mapping spaces (i.e., large M), and efficient mesh interpolation routines to speed up the evaluation of the objective function in (1).

Acknowledgments

The author acknowledges the support by European Union’s Horizon 2020 research and innovation programme under the Marie Skłodowska-Curie Actions, grant agreement 872442 (ARIA), and the support provided by Inria under the programme Exploratory Actions (project AM2OR, co-PI: Nicolas Barral). The author also thanks Prof. Angelo Iollo (Univ. Bordeaux, Inria), Dr. Pierre Mounoud (Univ. Bordeaux), Dr. Alberto Remigi (Safran Tech), and Prof. Masayuki Yano (University of Toronto) for fruitful discussions on various elements of the method.

A Proof of Proposition 2.1

We first state a number of preliminary results.

Proposition A.1. *Let $\Omega_p \subset \mathbb{R}^2$ be a polytope isomorphic to the unit ball. Consider the vector-valued function $\Phi : \Omega_p \rightarrow \mathbb{R}^2$ that satisfies (i) $\Phi \in C^1(\overline{\Omega}_p; \mathbb{R}^2)$; (ii) $|J(\Phi)(x)| = |\det(\nabla\Phi(x))| \geq \epsilon > 0$ for all $x \in \Omega_p$ and a given $\epsilon > 0$; (iii) $\Phi(\partial\Omega_p) \subseteq \partial\Omega_p$. Then, Φ is a bijection that maps Ω_p into Ω_p .*

Proof. This result is a variant of Proposition 2.1 in [27] for polytopes Ω_p isomorphic to the unit ball; the proof follows the exact same steps of the one in [27]; details are omitted. In [27] we assumed that Φ is of class C^1 in a δ -neighborhood of Ω_p ; since Ω_p is a Lipschitz domain, if Φ is of class C^1 up to the boundary, then there exists a C^1 extension of Φ to \mathbb{R}^2 (cf. [4, section 2.5]): we can thus replace the hypothesis (i) of [27, Proposition 2.1] with the hypothesis $\Phi \in C^1(\overline{\Omega}_p; \mathbb{R}^2)$. Furthermore, we replace $J(\Phi)(x) \geq \epsilon > 0$ for all $x \in \Omega_p$ with the more general assumption $|J(\Phi)(x)| \geq \epsilon > 0$: since $J(\Phi)$ is continuous, this condition means that $J(\Phi)$ is either strictly positive or strictly negative in Ω_p . \square

Lemma A.1. *Let $\Phi = \mathbf{i}d + \varphi$ be a $C^1(\overline{\Omega_p}; \mathbb{R}^2)$ such that $\varphi \cdot \mathbf{n}|_{\partial\Omega_p} = 0$. Then, $\Phi(\partial\Omega_p) = \partial\Omega_p$.*

Proof. It suffices to prove that each edge F is mapped in itself. Towards this end, we define the vertices x_1^y, x_2^y of F , the tangent and normal vectors $\mathbf{t}_f, \mathbf{n}_f$ and the parameterization $\gamma_f : [0, 1] \rightarrow F$ such that $\gamma_f(s) = x_1^y + s\|x_2^y - x_1^y\|_2 \mathbf{t}_f$. We also introduce the normal vectors $\mathbf{n}_f^-, \mathbf{n}_f^+$ of the neighboring edges that meet F at x_1^y, x_2^y , respectively.

We first observe that $\varphi_\delta(x_1^y) = \varphi_\delta(x_2^y) = 0$: since F meets with the neighboring edges, the pairs of normals $\mathbf{n}_f^-, \mathbf{n}_f$ and $\mathbf{n}_f^+, \mathbf{n}_f$ should be linearly independent (i.e., they should span \mathbb{R}^2); then, exploiting the continuity of φ_δ up to the boundary of Ω_p — and in particular on $\partial\Omega_p$ — we find $\varphi_\delta(x_1^y) \cdot \mathbf{n}_f^- = \varphi_\delta(x_1^y) \cdot \mathbf{n}_f = 0$ and $\varphi_\delta(x_2^y) \cdot \mathbf{n}_f = \varphi_\delta(x_2^y) \cdot \mathbf{n}_f^+ = 0$, which imply $\varphi_\delta(x_1^y) = \varphi_\delta(x_2^y) = 0$.

By contradiction, $\Phi_\delta(F) \not\subset F$. Given $x \in F$, we find

$$\varphi_\delta(x) = (\varphi_\delta(x) \cdot \mathbf{n}_f) \mathbf{n}_f + (\varphi_\delta(x) \cdot \mathbf{t}_f) \mathbf{t}_f = (\varphi_\delta(x) \cdot \mathbf{t}_f) \mathbf{t}_f$$

and thus $\Phi_\delta(\gamma_f(s)) = x_1^y + \alpha(s) \mathbf{t}_f$ with $\alpha(s) = (\Phi_\delta(\gamma_f(s)) - x_1^y) \cdot \mathbf{t}_f$. Since $\varphi_\delta(x_1^y) = \varphi_\delta(x_2^y) = 0$, we find $\alpha(0) = 0, \alpha(1) = \|x_2^y - x_1^y\|_2$; therefore, the condition $\Phi_\delta(F) \not\subset F$ implies $\alpha'(s^*) = \mathbf{t}_f^T \nabla \Phi_\delta(\gamma_f(s^*)) \mathbf{t}_f = 0$ for some $s^* \in [0, 1]$. Note that $\Phi_\delta(\gamma_f(s)) \cdot \mathbf{n}_f = x_1^y \cdot \mathbf{n}_f$ for any $s \in [0, 1]$; if we differentiate left- and right-hand sides of the previous identity with respect to s we obtain $\mathbf{n}_f^T \nabla \Phi_\delta(\gamma_f(s)) \mathbf{t}_f = 0$ for all $s \in [0, 1]$. Therefore, if we set $x^* = \gamma_f(s^*)$, we find $\nabla \Phi_\delta(x^*) \mathbf{t}_f = (\mathbf{t}_f^T \nabla \Phi_\delta(x^*) \mathbf{t}_f) \mathbf{t}_f + (\mathbf{n}_f^T \nabla \Phi_\delta(x^*) \mathbf{t}_f) \mathbf{n}_f = 0$, which implies that $\nabla \Phi_\delta$ is singular at x^* and thus $\min_{x \in \overline{\Omega_p}} J(\Phi_\delta) \leq J(\Phi_\delta)(x^*) = 0$. Contradiction. \square

Lemma A.2. *Let $\Omega = \Omega_{\text{ext}} \setminus \Omega_{\text{int}}$ be a regular polytope such that $\Omega_{\text{int}}, \Omega_{\text{ext}}$ are isomorphic to the unit ball. Let $\Phi^+ : \Omega \rightarrow \mathbb{R}^2$ and $\Phi^- : \Omega_{\text{int}} \rightarrow \mathbb{R}^2$ be C^1 maps that coincide on $\Gamma := \partial\Omega_{\text{int}}$ and satisfy $J(\Phi^+)(x) \geq \epsilon > 0$ for all $x \in \Omega$, $J(\Phi^-)(x) \geq \epsilon > 0$ for all $x \in \Omega_{\text{int}}$. Then, there exists a sequence $\{\Phi_j\}_j \subset C^1(\overline{\Omega}; \mathbb{R}^2)$ such that (i) $\Phi_j = \Phi$ on $\partial\Omega_{\text{ext}}$, (ii) $\lim_{j \rightarrow \infty} \|\Phi_j - \Phi\|_{L^\infty(\Omega_{\text{ext}})} = 0$, (iii) $\min_{x \in \overline{\Omega}} J(\Phi_j) \geq \frac{1}{2}\epsilon$ for $j = 1, 2, \dots$, where $\Phi : \Omega_{\text{ext}} \rightarrow \mathbb{R}^2$ is equal to Φ^+ in Ω and is equal to Φ^- in Ω_{int} .*

Proof. We define the piecewise-linear parameterization $\gamma : (0, 1) \rightarrow \Gamma$; we denote by \mathbf{t} the tangent vector to Γ , by \mathbf{n} the normal vector that points towards Ω , and by V_{int} the vertices of Ω on Γ ; $\text{dist}_H(A, B)$ is the Hausdorff distance between the sets A and B . Given $\delta > 0$, we define the set $V_{\text{int}, \delta} = \bigcup_{x \in V_{\text{int}}} \mathcal{B}_\delta(x)$, and the C^1 approximation Γ_δ of Γ such that $\text{dist}_H(\Gamma_\delta, \Gamma) \leq \delta$ and $\text{dist}_H(\Gamma_\delta \setminus V_{\text{int}, \delta}, \Gamma \setminus V_{\text{int}, \delta}) = 0$. Then, we introduce the C^1 parameterization $\gamma_\delta : (0, 1) \rightarrow \Gamma_\delta$, the corresponding unit normal \mathbf{n}_δ and the set $\Gamma_{\eta, \delta} = \{\gamma_\delta(u) + \eta v \mathbf{n}_\delta : v \in (-f(u), 1 - f(u)), u \in (0, 1)\}$, where $f : (0, 1) \rightarrow [0, 1]$ is a suitable function that will be introduced below.

Exploiting the previous definitions, we define $\psi_{\eta, \delta} : \mathbb{R}^2 \rightarrow [0, 1]$ such that (i) $\psi_{\eta, \delta}(\gamma_\delta(u) + \eta v \mathbf{n}_\delta) = \phi(v + f(u))$ for all $u \in (0, 1), v \in (-f(u), 1 - f(u))$, with $\phi(t) = -2t^3 + 3t^2$, (ii) $\psi_{\eta, \delta}|_{\Omega_{\text{ext}} \setminus \Gamma_{\eta, \delta}} = 1$, and (iii) $\psi_{\eta, \delta}|_{\Omega_{\text{int}} \setminus \Gamma_{\eta, \delta}} = 0$. It is straightforward to verify that $\psi_{\eta, \delta}$ is of class C^1 , and that

$$\nabla \psi_{\eta, \delta}(x) = \begin{cases} \frac{1}{\eta} (\alpha_{\psi, \delta}(x) \mathbf{n} + o(1)) & \forall x \in \Gamma_{\eta, \delta} \setminus V_{\text{int}, \delta}, \\ \mathcal{O} \left(\frac{\alpha_{\psi, \delta}(x)}{\eta} \mathbf{n}_\delta + \frac{\beta_{\psi, \delta}(x)}{\delta} \mathbf{t}_\delta \right) & \forall x \in V_{\text{int}, \delta}, \end{cases}$$

where $\alpha_{\psi, \delta}(x) \in (0, \max_{v \in \mathbb{R}} \phi'(v)) = (0, 3/2)$ and $\beta_{\psi, \delta}(x)$ belongs to a bounded interval that is independent of $\delta > 0$.

We define the positive vanishing sequences $\{\eta_j\}_j, \{\delta_j\}_j \subset \mathbb{R}_+$; for $j = 1, 2, \dots$, we introduce the function $\psi_j = \psi_{\eta_j, \delta_j}$ and the field $\Phi_j = (\Phi_e^+ - \Phi_e^-) \psi_j + \Phi_e^-$, where Φ_e^+, Φ_e^- are C^1 extensions of Φ^+, Φ^- to \mathbb{R}^2 (cf. [4, section 2.5]). Clearly, $\{\Phi_j\}_j$ satisfies the conditions (i) and (ii); furthermore, $J(\Phi_j) \geq \epsilon$ in $\Omega_{\text{ext}} \setminus \Gamma_{\eta_j, \delta_j}$; in the remainder, we prove that $J(\Phi_j) \geq \epsilon/2$ in $\Gamma_{\eta_j, \delta_j}$.

Let $x \in \Gamma_{\eta_j, \delta_j} \setminus V_{\text{int}, \delta_j}$. Since $\Phi^+ = \Phi^-$ on Γ , we have $(\nabla(\Phi_e^+ - \Phi_e^-)) \mathbf{t} = 0$ for all $x \in \Gamma$. We define $\mathbf{t}_\Phi = \frac{\nabla \Phi_e^+ \mathbf{t}}{\|\nabla \Phi_e^+ \mathbf{t}\|_2}$ and $\mathbf{n}_\Phi = [(\mathbf{t}_\Phi)_2, -(\mathbf{t}_\Phi)_1]$. Given $x \in \Gamma_{\eta_j, \delta_j}$, $x = \gamma(u) + \eta_j v \mathbf{n}$, we define $\bar{x} = \gamma(u)$ and $\bar{y} = \Phi_e^+(\bar{x}) = \Phi_e^-(\bar{x})$. Then,

$$\begin{aligned} \Phi_e^\pm(x) &\approx \bar{y} + \nabla \Phi_e^\pm(x - \bar{x}) = \bar{y} + \nabla \Phi_e^\pm \mathbf{t} \mathbf{t}^T (x - \bar{x}) + \nabla \Phi_e^\pm \mathbf{n} \mathbf{n}^T (x - \bar{x}) \\ &= \bar{y} + (\alpha \mathbf{t}_\Phi \mathbf{t}^T + \beta^\pm \mathbf{t}_\Phi \mathbf{n}^T + \gamma^\pm \mathbf{n}_\Phi \mathbf{n}^T) (x - \bar{x}), \end{aligned}$$

which implies $\nabla \Phi_e^\pm = \alpha \mathbf{t}_\Phi \mathbf{t}^T + \beta^\pm \mathbf{t}_\Phi \mathbf{n}^T + \gamma^\pm \mathbf{n}_\Phi \mathbf{n}^T$, where $\alpha, \beta^\pm, \gamma^\pm, \mathbf{t}_\Phi$ depend on \bar{x} . Exploiting the latter, we find

$$\begin{aligned} \nabla \Phi_j &= (\nabla \Phi_e^+ - \nabla \Phi_e^-) \psi_j + (\Phi_e^+ - \Phi_e^-) (\nabla \psi_j)^T + \nabla \Phi_e^- \\ &\approx \alpha \mathbf{t}_\Phi \mathbf{t}^T + (\beta^- + \llbracket \beta \rrbracket \psi_\eta) \mathbf{t}_\Phi \mathbf{n}^T + (\gamma^- + \llbracket \gamma \rrbracket \psi_\eta) \mathbf{n}_\Phi \mathbf{n}^T + v \alpha_\psi (\llbracket \beta \rrbracket \mathbf{t}_\Phi + \llbracket \gamma \rrbracket \mathbf{n}_\Phi) \mathbf{n}^T, \end{aligned}$$

for all $x \in \Gamma_\eta$. Since $\{\mathbf{t}, \mathbf{n}\}$ and $\{\mathbf{t}_\Phi, \mathbf{n}_\Phi\}$ are orthonormal bases of \mathbb{R}^2 , we must have

$$J(\Phi_\eta) = \alpha (\gamma^- + \llbracket \gamma \rrbracket) (\psi_\eta + v\alpha_\psi) + o(1).$$

Let α be positive; the case $\alpha < 0$ is analogous. If $\llbracket \gamma \rrbracket > 0$, we find

$$\gamma^- + \llbracket \gamma \rrbracket \left(\underbrace{\psi_\eta}_{\geq 0} + \underbrace{v}_{\geq -f(u)} \underbrace{\alpha_\psi}_{\leq 3/2} \right) \geq \gamma - \frac{3}{2} \llbracket \gamma \rrbracket f(u),$$

which exceeds $\gamma^-/2$ if $f(u) \leq \frac{\gamma^-}{3\llbracket \gamma \rrbracket}$. If $\llbracket \gamma \rrbracket < 0$, we find that $J(\Phi_\eta) \geq \alpha \frac{\gamma^\pm}{2}$ provided that $f(u) \geq 1 - \frac{\gamma^+}{3\llbracket \gamma \rrbracket}$. Note that for $\llbracket \gamma \rrbracket = 0$ the bounds reduce to $-\infty \leq f(u) \leq \infty$: we can hence find a smooth function f such that $J(\Phi_j) \geq \frac{\alpha}{2} \min\{\gamma^+, \gamma^-\} \geq \frac{\epsilon}{2}$.

Let $x \in \Gamma_{\eta_j, \delta_j} \cap V_{\text{int}, \delta_j}$; we assume that $\eta_j = \mathcal{O}(\delta_j)$ for $j = 1, 2, \dots$. Exploiting the same argument as before, we find $\nabla \Phi_e^+ = \nabla \Phi_e^-$ for $x \in V_{\text{int}}$. Therefore, by considering a Taylor expansion centered in $x \in V_{\text{int}}$, we find

$$\begin{aligned} \nabla \Phi_j &= (\nabla \Phi_e^+ - \nabla \Phi_e^-) \psi_j + (\Phi_e^+ - \Phi_e^-) (\nabla \psi_j)^T + \nabla \Phi_e^- \\ &= o(1)\mathcal{O}(1) + o(\delta)\mathcal{O}\left(\frac{\alpha_{\psi, \delta}(x)}{\eta} \mathbf{n}_\delta + \frac{\beta_{\psi, \delta}(x)}{\delta} \mathbf{n}_\delta\right) + \nabla \Phi_e^- \stackrel{(i)}{=} \nabla \Phi_e^- + o(1), \end{aligned}$$

which implies $J(\Phi_j) \gtrsim \epsilon$. In (i), we exploited the hypothesis $\eta_j = \mathcal{O}(\delta_j)$ for $j = 1, 2, \dots$ \square

Proof. (Proposition 2.1). Regular polytopes (cf. Definition 2.1) can be described as $\Omega_p = \Omega_{\text{ext}} \setminus \bigcup_{i=1}^N \Omega_{\text{int}, i}$ where $\Omega_{\text{int}, 1}, \dots, \Omega_{\text{int}, N}$ are pairwise disjoint polytopes that are compactly embedded in Ω_{ext} and $\Omega_{\text{ext}}, \Omega_{\text{int}, 1}, \dots, \Omega_{\text{int}, N}$ are isomorphic to the unit ball. Without loss of generality, we can hence prove the desired result for regular polytopes of the form $\Omega_p = \Omega_{\text{ext}} \setminus \Omega_{\text{int}}$.

Exploiting Lemma A.1, we find that $\Phi|_{\partial\Omega_{\text{int}}}$ is a diffeomorphism from $\partial\Omega_{\text{int}}$ in itself. Exploiting Cerf's theorem (see, e.g., [13]), we find that there exists a C^1 mapping $\Psi : \Omega_{\text{int}} \rightarrow \Omega_{\text{int}}$ such that $\Psi = \Phi$ on $\partial\Omega_{\text{int}}$ and $|J(\Psi)|$ does not vanish in $\bar{\Omega}_{\text{int}}$: exploiting the same argument as in Lemma A.2, we find that $\nabla \Psi = \nabla \Phi$ on the vertices of $\partial\Omega_{\text{int}}$; therefore, $J(\Psi)$ is strictly positive in $\bar{\Omega}_{\text{int}}$. We set $\epsilon = \{\inf_{x \in \Omega_p} J(\Phi), \inf_{x \in \Omega_{\text{int}}} J(\Psi)\}$. We now define the extended map $\Phi_{\text{ext}} : \Omega_{\text{ext}} \rightarrow \mathbb{R}^2$ that is equal to Φ in Ω_p and is equal to Ψ in Ω_{int} . Below, we prove that Φ_{ext} is a bijection in Ω_{ext} : since Ψ is bijective in Ω_{int} , this implies that Φ is bijective in Ω_p .

We introduce a sequence $\{\Phi_j\}_j \subset C^1(\bar{\Omega}_{\text{ext}}; \mathbb{R}^2)$ such that (i) $\Phi_j = \Phi$ on $\partial\Omega_{\text{ext}}$, (ii) $\lim_{j \rightarrow \infty} \delta_j := \|\Phi_j - \Phi_{\text{ext}}\|_{L^\infty(\Omega_{\text{ext}})} = 0$, (iii) $\min_{x \in \bar{\Omega}_{\text{ext}}} J(\Phi_j) \geq \frac{1}{2}\epsilon$ for $j = 1, 2, \dots$ (cf. Lemma A.2). For any $j > 0$, Φ_j satisfies the hypotheses of Proposition A.1: it is hence bijective in Ω_{ext} .

We can exploit the knowledge of $\{\Phi_j\}_j$ to prove that Φ_{ext} is surjective in Ω_{ext} . We have indeed that, for any $y \in \Omega_{\text{ext}}$,

$$\text{dist}(y, \Phi_{\text{ext}}(\Omega_{\text{ext}})) = \text{dist}(\Phi_j(x_j), \Phi_{\text{ext}}(\Omega_{\text{ext}})) \leq \text{dist}(\Phi_j(x_j), \Phi_{\text{ext}}(x_j)) \leq \delta_j,$$

where $x_j \in \Omega_{\text{ext}}$ is the preimage of y through Φ_j ; since the latter holds for any j , we must have $\text{dist}(y, \Phi_{\text{ext}}(\Omega_{\text{ext}})) = 0$.

By contradiction, assume that Φ_{ext} is not injective, that is, there exist $x, y \in \Omega_{\text{ext}}$ such that $\Phi_{\text{ext}}(x) = \Phi_{\text{ext}}(y)$. We distinguish between the case in which $x, y \in \partial\Omega_{\text{int}}$ and the case in which $x \notin \partial\Omega_{\text{int}}$: since $\Phi|_{\partial\Omega_{\text{int}}}$ is a diffeomorphism from $\partial\Omega_{\text{int}}$ in itself, the first scenario is impossible; we hence focus on the second case. We define the ball B_x of radius η centered in x ; recalling notation introduced in Lemma A.2, if η is sufficiently small, there exists $j_0 \in \mathbb{N}$ such that $\Gamma_{\eta_j, \delta_j} \cap B_x = \emptyset$ for all $j > j_0$. The latter implies that Φ_j is independent of j in B_x and thus there exists $c > 0$ such that $\|\Phi_j(x') - \Phi_j(x)\|_2 \geq c\eta$ for any $x' \in \partial B_x$ and $j > j_0$. The condition $\Phi(x) = \Phi(y)$ implies $\|\Phi_j(x) - \Phi_j(y)\|_2 \leq \delta_j$ and thus $\text{dist}(y, \Phi_j(B_x)) = 0$ for any j satisfying $\delta_j < c\eta$. Therefore, Φ_j is not a bijection. Contradiction. \square

References

- [1] J. H. Argyris, I. Fried, and D. W. Scharpf. The TUBA family of plate elements for the matrix displacement method. *The Aeronautical Journal*, 72(692):701–709, 1968.
- [2] N. Barral, T. Taddei, and I. Tifouti. Registration-based model reduction of parameterized pdes with spatio-parameter adaptivity. *arXiv preprint arXiv:2308.01773*, 2023.
- [3] T. Blickhan. A registration method for reduced basis problems using linear optimal transport. *arXiv preprint arXiv:2304.14884*, 2023.

- [4] A. Brudnyi and Y. Brudnyi. *Methods of geometric analysis in extension and trace problems: volume 1*, volume 102. Springer Science & Business Media, 2011.
- [5] V. Camion and L. Younes. Geodesic interpolating splines. In *International workshop on energy minimization methods in computer vision and pattern recognition*, pages 513–527. Springer, 2001.
- [6] Y. Cao, M. I. Miller, R. L. Winslow, and L. Younes. Large deformation diffeomorphic metric mapping of vector fields. *IEEE transactions on medical imaging*, 24(9):1216–1230, 2005.
- [7] J. S. Hesthaven and T. Warburton. *Nodal discontinuous Galerkin methods: algorithms, analysis, and applications*. Springer Science & Business Media, 2007.
- [8] A. Iollo and D. Lombardi. Advection modes by optimal mass transfer. *Physical Review E*, 89(2):022923, 2014.
- [9] A. Iollo and T. Taddei. Mapping of coherent structures in parameterized flows by learning optimal transportation with Gaussian models. *Journal of Computational Physics*, 471:111671, 2022.
- [10] M. Jacobs and F. Léger. A fast approach to optimal transport: The back-and-forth method. *Numerische Mathematik*, 146(3):513–544, 2020.
- [11] G. E. Karniadakis and S. Sherwin. *Spectral/hp element methods for computational fluid dynamics*. Oxford University Press on Demand, 2005.
- [12] S. G. Krantz and H. R. Parks. *The implicit function theorem: history, theory, and applications*. Springer Science & Business Media, 2002.
- [13] F. Laudenbach. About the diffeomorphisms of the 3-sphere and a famous theorem of Cerf ($\Gamma_4 = 0$). *arXiv preprint arXiv:2306.12837*, 2023.
- [14] J. Ma, J. Wu, J. Zhao, J. Jiang, H. Zhou, and Q. Z. Sheng. Nonrigid point set registration with robust transformation learning under manifold regularization. *IEEE transactions on neural networks and learning systems*, 30(12):3584–3597, 2018.
- [15] M. A. Mirhoseini and M. J. Zahr. Model reduction of convection-dominated partial differential equations via optimization-based implicit feature tracking. *Journal of Computational Physics*, page 111739, 2022.
- [16] R. Mojjani and M. Balajewicz. Arbitrary Lagrangian Eulerian framework for efficient projection-based reduction of convection dominated nonlinear flows. In *APS Division of Fluid Dynamics Meeting Abstracts*, pages M1–008, 2017.
- [17] I. Mozolevski, E. Süli, and P. R. Bösing. hp-version a priori error analysis of interior penalty discontinuous galerkin finite element approximations to the biharmonic equation. *Journal of Scientific Computing*, 30(3):465–491, 2007.
- [18] A. Myronenko and X. Song. Point set registration: Coherent point drift. *IEEE transactions on pattern analysis and machine intelligence*, 32(12):2262–2275, 2010.
- [19] F. Nicoud and F. Ducros. Subgrid-scale stress modelling based on the square of the velocity gradient tensor. *Flow, turbulence and Combustion*, 62(3):183–200, 1999.
- [20] P.-O. Persson and J. Peraire. Sub-cell shock capturing for discontinuous Galerkin methods. In *44th AIAA aerospace sciences meeting and exhibit*, page 112, 2006.
- [21] G. Peyré and M. Cuturi. Computational optimal transport: With applications to data science. *Foundations and Trends® in Machine Learning*, 11(5-6):355–607, 2019.
- [22] M. Ruzhansky and M. Sugimoto. On global inversion of homogeneous maps. *Bulletin of Mathematical Sciences*, 5(1):13–18, 2015.
- [23] N. Sarna and P. Benner. Data-driven model order reduction for problems with parameter-dependent jump-discontinuities. *Computer Methods in Applied Mechanics and Engineering*, 387:114168, 2021.
- [24] G. R. Shubin, A. Stephens, and H. M. Glaz. Steady shock tracking and Newton’s method applied to one-dimensional duct flow. *Journal of Computational Physics*, 39(2):364–374, 1981.
- [25] L. Sirovich. Turbulence and the dynamics of coherent structures. I. Coherent structures. *Quarterly of applied mathematics*, 45(3):561–571, 1987.

- [26] M. L. Staten, S. J. Owen, S. M. Shontz, A. G. Salinger, and T. S. Coffey. A comparison of mesh morphing methods for 3D shape optimization. In *Proceedings of the 20th international meshing roundtable*, pages 293–311. Springer, 2012.
- [27] T. Taddei. A registration method for model order reduction: data compression and geometry reduction. *SIAM Journal on Scientific Computing*, 42(2):A997–A1027, 2020.
- [28] T. Taddei. An optimization-based registration approach to geometry reduction. *arXiv preprint arXiv:2211.10275*, 2022.
- [29] T. Taddei and L. Zhang. Registration-based model reduction in complex two-dimensional geometries. *Journal of Scientific Computing*, 88(3):79, 2021.
- [30] T. Taddei and L. Zhang. Space-time registration-based model reduction of parameterized one-dimensional hyperbolic pdes. *ESAIM: Mathematical Modelling and Numerical Analysis*, 55(1):99–130, 2021.
- [31] P. Tonon, R. A. K. Sanches, K. Takizawa, and T. E. Tezduyar. A linear-elasticity-based mesh moving method with no cycle-to-cycle accumulated distortion. *Computational Mechanics*, 67(2):413–434, 2021.
- [32] S. Volkwein. Model reduction using proper orthogonal decomposition. *Lecture Notes, Institute of Mathematics and Scientific Computing, University of Graz*. see <http://www.uni-graz.at/imawww/volkwein/POD.pdf>, 1025, 2011.
- [33] H. Wendland. *Scattered data approximation*, volume 17. Cambridge university press, 2004.
- [34] M. J. Zahr and P.-O. Persson. An optimization-based approach for high-order accurate discretization of conservation laws with discontinuous solutions. *Journal of Computational Physics*, 365:105–134, 2018.
- [35] M. J. Zahr and P.-O. Persson. An r-adaptive, high-order discontinuous Galerkin method for flows with attached shocks. In *AIAA Scitech 2020 Forum*, page 0537, 2020.
- [36] M. J. Zahr, A. Shi, and P.-O. Persson. Implicit shock tracking using an optimization-based high-order discontinuous Galerkin method. *Journal of Computational Physics*, 410:109385, 2020.